# Microglial SIRPα regulates the emergence of CD11c$^+$ microglia and demyelination damage in white matter

Miho Sato-Hashimoto[1], Tomomi Nozu[1], Riho Toriba[1], Ayano Horikoshi[1], Miho Akaike[1], Kyoko Kawamoto[1], Ayaka Hirose[1], Yuriko Hayashi[1], Hiromi Nagai[1], Wakana Shimizu[1], Ayaka Saiki[1], Tatsuya Ishikawa[2], Ruwaida Elhanbaly[2,3], Takenori Kotani[4], Yoji Murata[4], Yasuyuki Saito[4], Masae Naruse[5], Koji Shibasaki[5], Pre-Arne Oldenborg[6], Steffen Jung[7], Takashi Matozaki[4], Yugo Fukazawa[2], and Hiroshi Ohnishi[1,*]

[1]Department of Laboratory Sciences, Gunma University Graduate School of Health Sciences, Gunma 371-8514, Japan

[2]Division of Brain Structure and Function, Life Science Innovation Center, Research Center for Child Mental Development, Faculty of Medical Sciences, University of Fukui, Fukui 910-1193, Japan

[3]Department of Anatomy, Histology and Embryology, Faculty of Veterinary Medicine, Assiut University, Assiut-71526, Egypt

[4]Division of Molecular and Cellular Signaling, Department of Biochemistry and Molecular Biology, Kobe University Graduate School of Medicine, Kobe 650-0017, Japan

[5]Department of Molecular and Cellular Neurobiology, Gunma University Graduate School of Medicine, Gunma 371-8511, Japan

[6]Department of Integrative Medical Biology, Section for Histology and Cell Biology, Umeå University, SE-901 87 Umeå, Sweden

[7]Department of Immunology, The Weizmann Institute of Science, Rehovot 76100, Israel

*Corresponding author: ohnishih@gunma-u.ac.jp (H. Ohnishi).

**Abstract**

A characteristic subset of microglia expressing CD11c appears in response to brain damage. However, the functional role of CD11c$^+$ microglia, as well as the mechanism of its induction, are poorly understood. Here we report that the genetic ablation of signal regulatory protein α (SIRPα), a membrane protein, induced CD11c$^+$ microglia in the brain white matter. Mice lacking CD47, a physiological ligand of SIRPα, and microglia-specific SIRPα knockout mice exhibited the same phenotype, suggesting the interaction between microglial SIRPα and CD47 on neighbouring cells suppressed the emergence of CD11c$^+$ microglia. A lack of SIRPα did not cause detectable damage in the white matter, but resulted in the increased expression of genes characteristic of the repair phase after demyelination. In addition, cuprizone-induced demyelination was alleviated by the microglia-specific ablation of SIRPα. Thus, microglial SIRPα suppresses the induction of CD11c$^+$ microglia that have the potential to accelerate the repair of damaged white matter.

42 **Introduction**

43 Microglia constantly survey the microenvironment of the brain. When microglia
44 encounter tissue damage, they become activated, produce multiple humoral factors and
45 show enhanced phagocytic activity; microglia thus play a central role in the removal
46 and repair of damaged tissues (Kettenmann, Hanisch, Noda, & Verkhratsky, 2011).
47 However, the excessive activation of microglia results in the progression of
48 inflammation and tissue degeneration, which is harmful to the brain environment
49 (Kettenmann et al., 2011). The activation of microglia has been reported in various
50 neurodegenerative diseases and brain injuries, including Alzheimer's disease (AD),
51 amyotrophic lateral sclerosis (ALS), and demyelinating diseases (Chiu et al., 2013;
52 Holtman et al., 2015; Kamphuis, Kooijman, Schetters, Orre, & Hol, 2016; Remington,
53 Babcock, Zehntner, & Owens, 2007; Wang et al., 2015). In animal models of these
54 disorders, a characteristic subset of microglia that express integrin αX or CD11c, a
55 marker of murine peripheral dendritic cells and selected macrophages, appear in the
56 affected brain regions. The expression of CD11c is a marker for "primed" microglia that
57 are not fully activated but rather are in a pre-activation state (Holtman et al., 2015;
58 Norden & Godbout, 2013). $CD11c^+$ microglia were also reported during postnatal
59 development and normal aging (Bulloch et al., 2008; Kaunzner et al., 2012). In both
60 cases, $CD11c^+$ microglia characteristically appeared in the brain white matter, where
61 myelin construction during the late developmental stage (Baumann & Pham-Dinh,
62 2001) or accumulation of damaged myelin debris during aging were remarkable
63 (Safaiyan et al., 2016). It was also shown that demyelination markedly induced $CD11c^+$
64 microglia, even in the adult brain (Remington et al., 2007), which was suppressed in
65 mutant mice lacking Trem2 or Cx3Cr1 (Lampron et al., 2015; Poliani et al., 2015), i.e.
66 functional molecules that promote phagocytosis. Of note, the clearance of myelin debris
67 was markedly impaired in these mutant mice (Cantoni et al., 2015; Lampron et al.,
68 2015; Poliani et al., 2015). $CD11c^+$ microglia also accumulate around amyloid plaques

69 in an AD mouse model with gene expression patterns indicating an enhanced capacity
70 for phagocytosis (Kamphuis et al., 2016; Wang et al., 2015). Phagocytic ability of
71 CD11c$^+$ microglia thus might contribute to the removal and repair of damaged tissues.
72 However, the physiological roles of CD11c$^+$ microglia, as well as the mechanisms
73 controlling the induction of CD11c$^+$ microglia, are not fully understood.
74 SIRPα (CD172a) is a membrane protein highly expressed in macrophages and
75 dendritic cells. The extracellular region of SIRPα specifically interacts with another
76 membrane protein CD47 to promote cell–cell contact signals (Matozaki, Murata,
77 Okazawa, & Ohnishi, 2009). Interactions between SIRPα on phagocytic cells and CD47
78 on phagocytosed targets, such as erythrocytes, cancer cells, and apoptotic cells, act as a
79 "don't eat me" signal and thereby control erythrocyte homeostasis, elimination of
80 cancer cells, and the formation of arteriosclerotic plaques (Chao et al., 2011;
81 Ishikawa-Sekigami et al., 2006; Kojima et al., 2016; Willingham et al., 2012). In the
82 brain, SIRPα and CD47 are abundantly expressed on neurons (Ohnishi et al., 2010), and
83 SIRPα is also expressed on microglia (Gitik, Liraz-Zaltsman, Oldenborg, Reichert, &
84 Rotshenker, 2011). It is assumed that SIRPα on microglia interacts with neuronal CD47
85 to suppress microglial activation (Saijo & Glass, 2011), because SIRPα contains an
86 immunoreceptor tyrosine-based inhibitory motif (ITIM) in its cytoplasmic region
87 (Barclay & Hatherley, 2008; Matozaki et al., 2009). However, direct *in vivo* evidence
88 supporting this model is missing. Here, we analysed the role of SIRPα in the control of
89 microglial activation using CD47-SIRPα signal-deficient mice and define a critical
90 microglia control module. Specifically, our results establish that SIRPα on microglia
91 controls cell activation through the interaction with its ligand CD47 and negatively
92 regulates the induction of CD11c$^+$ microglia in the white, but not grey matter, which
93 have the potential to support the repair of damaged myelin.

94 **Results**

95 ***Emergence of CD11c$^+$ microglia in the brain white matter of SIRPα-deficient mice***

96 To examine the role of SIRPα in microglial activation, brains of SIRPα knockout (KO)
97 mice were subjected to immunohistochemical analysis using antibodies specific to Iba1,
98 a microglia marker, and to CD68, a marker for phagocytically active microglia (**Figure**
99 **1A**). In the brains of SIRPα KO mice, numbers of Iba1$^+$ as well as Iba1$^+$/CD68$^+$ cells
100 were significantly increased in the white matter, such as the fimbria, compared with
101 wild-type (WT) control mice, suggesting the activation of microglia in these regions
102 (**Figures 1A and 1B**). Activation of microglia in the white matter was similar to the
103 phenotype reported in aged mice, in which numbers of CD11c$^+$ microglia were reported
104 to be increased (Kaunzner et al., 2012). Next we examined the effect of the genetic
105 ablation of SIRPα on the expression of CD11c on microglia by using CD11c-EYFP
106 transgenic (Tg) mice (Lindquist et al., 2004), in which the expression of CD11c is
107 detected with a reporter gene. In SIRPα KO:CD11c-EYFP Tg mice, Iba1$^+$ cells and
108 EYFP$^+$ cells were markedly increased in the white matter, including the corpus callosum,
109 external capsule, fimbria, and internal capsule, compared with control
110 SIRPα$^{+/+}$:CD11c-EYFP Tg mice (**Figure 1C**). Most EYFP$^+$ cells in the white matter of
111 SIRPα KO mice were Iba1 positive, suggesting they were CD11c$^+$ microglia (**Figure**
112 **1D *lower panels***). In contrast, the EYFP signal was barely detected in the grey matter of
113 both genotypes (**Figure 1D *upper panels***). The white matter-specific emergence of
114 Iba1$^+$/CD11c$^+$ cells was also confirmed by using a specific antibody to CD11c in the
115 brain or spinal cord of SIRPα KO mice (**Figure 2A and 2B**).

116 Demyelination damage causes microglia activation and an increase in the
117 number of CD11c$^+$ microglia in the white matter of the brain (Remington et al., 2007).
118 Thus, we examined the structural integrity of myelin in SIRPα KO mice. Although a
119 marked increase of CD11c$^+$ cells was observed in the anterior commissure of SIRPα
120 KO mice, no appreciable demyelination was evident by immunostaining for myelin

121 basic protein (MBP) (**Figure 2C**). Myelination in the corpus callosum and fimbria were
122 also normal in SIRPα KO mice when examined by myelin staining with a
123 gold-phosphate complex (Black-Gold II) (**Figure 2D**).
124
125 ***Increased expression of innate immune molecules in CD11c$^+$ microglia in the brain***
126 ***of SIRPα-deficient mice and aged mice***
127 We then examined the characteristics of the CD11c$^+$ microglia. Microglia were isolated
128 from the spinal cord of SIRPα KO and control WT mice, and the CD11b$^+$/CD45$^{dim/lo}$
129 fraction was analysed by flow cytometry (**Figures 3A-3C**). The yield of microglia from
130 SIRPα KO mice was significantly higher than that from control mice [8.12 ± 0.47 and
131 4.57 ± 0.97 ×10$^4$ cells/mouse, respectively; mean ± SEM ($n$ = 5 animals), $P$ = 0.01152
132 (Student's $t$-test)], indicating an increased number of microglia in the spinal cord of
133 SIRPα KO mice. As expected, expression of SIRPα was completely abolished in
134 microglia prepared from SIRPα KO mice (**Figure 3A**). Consistent with the results from
135 immunohistochemical analysis, CD11c$^+$/CD11b$^+$/CD45$^{dim/lo}$ microglia were increased in
136 SIRPα KO mice when compared with control WT mice (**Figure 3B**). Forward (FSC)
137 and side (SSC) scatter distribution of CD11c$^+$ microglia were similar to that of CD11c$^-$
138 microglia in the SIRPα KO mice, suggesting cell size and granularity (complexity)
139 were comparable between the two subsets (**Figure 3—figure supplement 1**). CD11c$^+$
140 microglia expressed higher levels of innate immune molecules, including CD14,
141 Dectin-1, and CD68 compared with CD11c$^-$ microglia in SIRPα KO mice (**Figure 3C**).
142 To compare CD11c$^+$ microglia in SIRPα KO mice with those in aged WT mice
143 (Bulloch et al., 2008; Kaunzner et al., 2012), microglia isolated from adult (16–18
144 weeks of age) and aged (69–105 weeks of age) WT mice were analysed in the same
145 manner (**Figure 3D-F**). The expression levels of SIRPα in microglia were comparable
146 between aged and adult mice (**Figure 3D**). Similar to SIRPα KO mice, CD11c$^+$
147 microglia were increased in aged mice compared with adult mice (**Figure 3E**). In

148 addition, CD11c$^+$ microglia in the aged mice expressed higher levels of CD14, Dectin-1,
149 and CD68 compared with CD11c$^-$ microglia as in SIRPα KO mice (**Figure 3F**).
150 To address the effect of the increase of CD11c$^+$ microglia on inflammatory
151 responses, we examined the expression of pro- and anti-inflammatory cytokines in the
152 brain and spinal cord by quantitative PCR analysis. Among the examined cytokines
153 (TNF-α, IL-1β, IL-6, IL-10 and TGF-β), the expression of TNF-α was increased in
154 SIRPα KO as compared to WT mice (**Figure 3—figure supplement 2**).
155
156 ***Induction of CD11c$^+$ microglia in the white matter of CD47-deficient mice***
157 To address the mechanism involved in the regulation of microglia activation by SIRPα,
158 we examined the effect of the genetic ablation of CD47, a membrane protein and SIRPα
159 ligand (Matozaki et al., 2009). In the brain of CD47 KO mice, CD11c$^+$ microglia were
160 increased in the white matter as observed for the brains of SIRPα KO mice (**Figure 4A**).
161 The number of Iba1$^+$ microglia was increased more than 2.5-fold in the hippocampal
162 fimbria, and about 70% of the Iba1$^+$ microglia expressed CD11c (**Figure 4B**). Flow
163 cytometric analysis showed that CD47 was expressed in WT microglia suggesting
164 possible microglia-microglia communication through CD47-SIRPα interaction.
165 Expression CD47 was completely absent in CD47 KO mice and the expression of
166 SIRPα was markedly increased in CD47 KO microglia (**Figure 4C**). Similar to SIRPα
167 KO mice, the yield of microglia from CD47 KO mice was increased compared with WT
168 mice [7.65 ± 0.91 and 3.34 ± 0.84 $\times 10^4$ cells/head, respectively; mean ± SEM ($n$ = 5
169 animals), $P$ = 0.00866 (Student's $t$-test)].
170
171 ***Increased expression of genes for the repair of damaged myelin in CD47-deficient***
172 ***mice***
173 To address the impact of the emergence of activated CD11c$^+$ microglia on the brain
174 environment, we compared the gene expression in the white matter (optic nerve and

175 optic tract) between CD47 KO mice and WT control mice by microarray transcriptome
176 analysis. Expression of total 14,875 genes was detected in both or either of the
177 genotypes. Among them, 594 and 548 genes were markedly (> 2-fold) increased and
178 decreased, respectively, in CD47 KO mice when compared with WT mice
179 (**Supplementary file 1**). Pathway analysis with Database for Annotation, Visualization
180 and Integrated Discovery (DAVID) ver. 6.8 (https://david.ncifcrf.gov/) (Huang,
181 Sherman, & Lempicki, 2009a, 2009b) suggested that genes increased in the white
182 matter of CD47 KO mice were significantly enriched in pathways such as infectious
183 diseases, phagocytosis, and immune responses, likely reflecting the activation of
184 microglia (**Figure 5A**). In contrast, genes decreased in CD47 KO mice were mostly
185 enriched in pathways for neuronal ligand-receptor interaction, and were also enriched in
186 pathways such as calcium signaling pathway and neuronal synapses (**Figure 5B**).
187 Consistent with the results of immunohistochemical and flow cytometric
188 analyses, the expression of *ItgaX* (CD11c), *Clec7a* (Dectin-1), *Cd68*, and *Cd14* were
189 markedly increased (> 2-fold: Log2 ratio > 1) in the white matter of CD47 KO mice
190 compared with WT mice (**Figure 5C**). In contrast, expression of the microglial markers
191 *Aif1* (Iba1) and *ItgaM* (CD11b), was only moderately increased (< 2-fold). Thus, the
192 marked increase in the expressions of CD11c and the other molecules was likely related
193 to the characteristic change in the mutant microglia (or other cells) in the white matter,
194 rather than to the increased number of microglia. Quantitative PCR analysis of selected
195 genes (*ItgaX*, *Igf1*, *Trem2*, *Ccl3*), which were increased in the microarray analysis, also
196 showed significant induction (**Figure 5—figure supplement 1**). We noted that several
197 transcripts reported to be increased in microglia during the repair of damaged myelin
198 (Holtman et al., 2015; Olah et al., 2012; Poliani et al., 2015; Selvaraju et al., 2004) were
199 markedly increased (> 2-fold) in the white matter of CD47 KO mice (**Figure 5C**).
200 These included *ItgaX*, *Lgals3*, and *Clec7a*, markers of primed microglia; *Lpl*, *Apoc1*,
201 and *Ch25h*, molecules for lipid transport; *Mmp12*, a tissue remodelling factor; *Igf1*, and

202 *Spp1*, trophic factors promoting oligodendrocyte differentiation; and *Cst7* (Cystatin F),
203 a cysteine proteinase inhibitor. We also found that the positive regulators of microglia
204 phagocytosis, *Trem2*, *DAP-12*, and *Cx3cr1* (Lampron et al., 2015; Poliani et al., 2015),
205 were increased in the white matter of the mutant mice.

206 We next examined the gene expression in the brain mononuclear cells, in
207 which microglia were enriched. Expression of total 16,544 genes was detected in both
208 or either of CD47 KO and WT control cells. Among them, 1,323 and 2,286 genes were
209 markedly (> 2-fold) increased and decreased, respectively, in the CD47 KO cells
210 (**Supplementary file 2**). Genes increased in CD47 KO brain cells were significantly
211 enriched in pathways for T cell receptor signal, axon guidance, proteoglycans in cancer,
212 TNF signal, and NF-κ B signal (**Figure 5A**); genes decreased in CD47 KO brain cells
213 were enriched in cancer associated pathways including Wnt, Hippo, and Rap1 signalling,
214 as well as cardiomyopathy (**Figure 5B**).

215 Comparison of array data revealed 32 and 55 genes that were commonly
216 increased and decreased (> 2-fold), respectively, in both the white matter and the brain
217 mononuclear cells of CD47 KO mice (**Figure 5—figure supplement 2**). Shared
218 induced genes included myelin-repair related genes, such as *ItgaX*, *Igf1*, *Lpl*, *Apoc1*,
219 *Ch25h*, *Mmp12*, *Spp1*, and *Cst7* (**Figure 5C**). The expression of *Clec7a*, *CD68*, *Trem2*,
220 and *Cx3cr1*, which were markedly increased in the white matter of CD47 KO mice,
221 showed only moderate (< 2-fold) increase in the brain mononuclear cells (**Figure 5C**).
222 Substantially higher expression of these genes in microglia might mask the increased
223 expression of these genes in the limited CD11c$^+$ subset that was only ~5 % of the total
224 microglia when prepared from the whole brain of CD47 KO mice (data not shown).
225

226 ***Induction of CD11c$^+$ microglia in the brain white matter of microglia-specific***
227 ***SIRPα-deficient mice***

228 To examine the cell type involved in the suppression of CD11c$^+$ microglia by SIRPα,
229 we analysed microglia-specific SIRPα conditional KO (cKO) mice that were generated
230 by crossing SIRPα-flox mice (Washio et al., 2015) and Cx3cr1-CreER$^{T2}$ mice to
231 achieve microglia-specific gene targeting (Goldmann et al., 2013; Safaiyan et al., 2016;
232 Wolf, Yona, Kim, & Jung, 2013). Flow cytometric analysis revealed that greater than
233 98% of microglia were SIRPα negative in the brain of tamoxifen-treated
234 SIRPα$^{fl/fl}$:Cx3cr1-CreER$^{T2}$ mice (**Figure 6A**), and the numbers of Iba1$^+$ and
235 Iba1$^+$/CD11c$^+$ microglia were increased in the hippocampal fimbria of these cKO mice
236 (**Figures 6B and 6C**). These data suggest that a lack of the interaction between SIRPα
237 on microglia and CD47 on neighbouring cells is the primary cause for the induction of
238 CD11c$^+$ microglia in CD47-SIRPα signal-deficient mice. We also analyzed CD11c$^+$
239 cell-specific SIRPα cKO mice (Washio et al., 2015). However, CD11c$^+$ microglia were
240 not increased in these mutant mice (**Figure 6—figure supplement 1**), suggesting that a
241 lack of SIRPα in the resident CD11c$^+$ microglia, a small subset of microglia in normal
242 mouse brain (Bulloch et al., 2008), did not cause the expansion of these cells.
243
244 ***Alleviation of cuprizone-induced demyelination in the brain white matter of***
245 ***microglia-specific SIRPα-deficient mice***
246 Although myelin damage induces CD11c$^+$ microglia (Remington et al., 2007),
247 demyelination was not observed in SIRPα total KO mice by light microscopy (**Figures**
248 **2C and 2D**). We examined the myelin structure again in microglia-specific cKO mice
249 by electron microscopy (**Figures 6D and 6E**). In the cross section of the anterior
250 commissure, the frequency of myelinated axons and the g-ratio (the ratio of the inner
251 axonal diameter to the total outer diameter) were comparable between SIRPα cKO and
252 control mice [frequency of myelinated axons: 34.3 ± 4.37% for control (n = 3), 36.3 ±
253 4.18% for cKO (n = 3), $P$ = 0.757, Student's $t$-test: g-ratio: 0.63 ± 0.025 for control (n =

254 3), 0.657 ± 0.009 for cKO (n = 3), $P = 0.374$, Student's *t*-test], suggesting the myelin
255 structure was normal in the mutant mice.
256 We further examined the progression of white matter damage in
257 microglia-specific SIRPα cKO mice undergoing cuprizone (Cpz)-induced
258 demyelination (Gudi, Gingele, Skripuletz, & Stangel, 2014; Norkute et al., 2009).
259 Feeding with Cpz, a copper chelator, for 5 weeks (wks), induced demyelination
260 accompanied by the robust accumulation of microglia (microgliosis) in white matter
261 regions including the hippocampal alveus and corpus callosum in control mice as
262 previously reported (**Figure 7A**) (Gudi et al., 2014; Norkute et al., 2009). At the site of
263 microgliosis, $CD11c^+$/$Iba1^+$ microglia were markedly increased, even in control mice
264 (**Figure 7A**). In SIRPα cKO mice, demyelination as well as microgliosis was
265 significantly reduced after the same treatment (**Figures 7A-7C**). At an early stage of
266 Cpz treatment (after 3 wks feeding with Cpz), demyelination was not observed in
267 control or SIRPα cKO mice (**Figure 7A**), but abnormally strong immunoreactivity of
268 MBP was observed (**Figure 7A**). This was probably related to myelin damage, because
269 the epitope of the anti-MBP antibody we used (DENPVV) is similar to that of a myelin
270 damage-detectable antibody (QDENPVV) (Matsuo et al., 1998). Consistently,
271 significant microgliosis as well as an increase in $CD11c^+$ cells were observed in both
272 genotypes after 3 wks feeding with Cpz (**Figures 7A and 7C**). At this stage, the area of
273 microgliosis was significantly larger in SIRPα cKO mice compared with control mice
274 (**Figures 7A and 7C**). The repair of demyelination was observed after feeding with
275 normal chow for 2 wks (**Figure 7A)**. Microgliosis was still present in both genotypes at
276 this time point but was significantly smaller in SIRPα cKO mice compared with control
277 mice (**Figures 7A and 7C**). In the white matter, including the corpus callosum and
278 alveus, the number of cells expressing $Olig2^+$, an oligodendrocyte progenitor and
279 lineage undergoing terminal differentiation into mature olidodendrocytes (Nishiyama,
280 Komitova, Suzuki, & Zhu, 2009), was significantly decreased at 3 wks of Cpz feeding,

281 suggesting demyelination was preceded by the loss of oligodendrocytes (**Figures 7A**
282 **and 7D**). The number of Olig2$^+$ cells was increased at 5 wks of Cpz treatment and
283 recovered to normal levels after another 2 wks feeding with normal chow (**Figures 7A**
284 **and 7D**). Throughout the de- and re-myelination process, no significant differences in
285 the number of Olig2$^+$ cells were noted between control and SIRPα cKO mice (**Figures**
286 **7A and 7D**).

287 **Discussion**

288 Cell–cell interactions between SIRPα on microglia and CD47 on neurons were
289 proposed to suppress the activation of microglia (Ransohoff & Cardona, 2010).
290 However, direct evidence for the function of this module in physiological context has
291 not been provided. In this study, we demonstrated that SIRPα is a key molecule for the
292 suppression of microglia activation *in vivo*. Molecules other than CD47, such as
293 surfactant protein-A and -D (SP-A, -D), have also been reported as SIRPα ligands
294 (Matozaki et al., 2009). However, we found that CD47 KO mice exhibited the same
295 phenotype as SIRPα KO mice suggesting that the CD47-SIRPα interaction is indeed
296 important for the suppression of microglia activation in the brain. In addition,
297 microglia-specific SIRPα cKO mice also exhibited the same phenotype. Therefore,
298 SIRPα expressed on microglia directly control microglia activation and the induction of
299 $CD11c^+$ microglia *in vivo*. The emergence of $CD11c^+$ microglia in the brains of
300 microglia-specific SIRPα cKO mice establishes that $CD11c^+$ microglia are derived from
301 resident microglia in the brain, and not recruited monocytes that are spared in the
302 TAM-induced system (Goldmann et al., 2013; Safaiyan et al., 2016; Wolf et al., 2013).
303 The characteristics of $CD11c^+$ microglia in our mutant mice were similar to that of
304 "primed microglia" that have been observed in aging and neurodegenerative diseases
305 (Holtman et al., 2015); thus, SIRPα is a possible key component regulating microglia
306 priming *in vivo*.

307 We found that the cell-surface expression of SIRPα was significantly
308 increased in CD47 KO mice. It is likely that the binding of CD47 destabilises SIRPα
309 molecules on microglia in the brain of WT mice, because our previous study suggested
310 that the interaction between CD47 and SIRPα induced endocytosis of the CD47-SIRPα
311 complex in CHO cells (Kusakari et al., 2008). It remains unclear which cell type
312 expressed CD47 that contributed to the suppression of $CD11c^+$ microglia. It was
313 proposed that CD47 expressed on neurons suppresses the activation of microglia

314 through interactions with SIRPα (Ransohoff & Cardona, 2010). An *in vitro* study
315 suggested that CD47 on myelin sheets interacted with SIRPα and suppressed microglial
316 phagocytosis (Gitik et al., 2011). Another study reported that direct cell–cell contact
317 between astrocytes and microglia suppressed the expression of CD11c on microglia
318 (Acevedo, Padala, Ni, & Jonakait, 2013). Thus, CD47 on oligodendrocytes or astrocytes
319 may also participate in the suppression of microglia activation. Finally, we showed that
320 microglia themselves express CD47 suggesting possible microglia-microglia interaction
321 through CD47-SIRPα signal. Further research with cell type-specific CD47 conditional
322 KO mice are required to clarify which cell type is involved in the CD47 mediated
323 effects.

324 $CD11c^+$ microglia are increased during neurodegenerative damage as well as
325 in aging and postnatal development of normal brain (Bulloch et al., 2008; Kaunzner et
326 al., 2012). We confirmed that $CD11c^+$ microglia in SIRPα KO mice had elevated
327 expressions of innate immune molecules including CD14, Dectin-1, and CD68, those
328 are characteristic of $CD11c^+$ microglia in WT aged mice. This suggested that the
329 phenotype in the mutant mice was similar to normal biological responses in the aged
330 brain. Although the maturation-dependent down regulation of CD47 was shown in
331 hematopoietic stem cells (Jaiswal et al., 2009), the age-dependent reduction of CD47
332 has not been reported in the brain. In addition, our data suggested that the cell surface
333 expression of SIRPα was not decreased in microglia from aged mice. Thus, the
334 age-dependent dysfunction of CD47-SIRPα signals was unlikely. The increase of
335 $CD11c^+$ microglia in aged brains may be explained by the age-dependent accumulation
336 of tissue damage that stimulates microglia activation beyond the suppressive ability of
337 SIRPα.

338 We demonstrated that $CD11c^+$ microglia were specifically increased in the
339 white matter of mutant mice. Thus, the white matter may contain an endogenous factor
340 that promotes the induction of $CD11c^+$ microglia in mutant mice. One potential

341 candidate is myelin. As reported (Poliani et al., 2015), CD11c$^{+}$ microglia were increased
342 in control SIRPα$^{+/+}$ mice after Cpz treatment. Thus, myelin damage effectively induces
343 CD11c$^{+}$ microglia even in the control mice. This suggests that myelin degradation
344 products during homeostatic turnover of the myelin structure might stimulate the
345 induction of CD11c$^{+}$ microglia in the CD47-SIRPα signal-deficient mice, while the
346 effect of such homeostatic degradation of myelin may be suppressed by SIRPα in the
347 normal mouse brain. Enhanced phagocytosis of myelin components by microglia may
348 be involved in the induction of CD11c$^{+}$ microglia in our mutant mice, because SIRPα
349 negatively regulated phagocytosis in macrophages (Matozaki et al., 2009). CD11c$^{+}$
350 microglia in SIRPα-deficient mice expressed CD68, a phagocytic marker, supporting
351 the notion that phagocytic activity was increased in these cells. Several studies have
352 suggested the importance of myelin phagocytosis by microglia for the induction of
353 CD11c$^{+}$ microglia during demyelination or aging. The myelin damage-dependent
354 induction of CD11c$^{+}$ microglia was markedly suppressed in mutant mice lacking Trem2,
355 a phagocytic receptor (Poliani et al., 2015). The emergence of CD11c$^{+}$ microglia during
356 demyelination was also suppressed in Cx3cr1 KO mice, in which the phagocytosis of
357 myelin debris by microglia was severely impeded (Lampron et al., 2015). In the brain of
358 aged mice, the accumulation of myelin debris and phagocytosis of such components by
359 microglia were increased in the white matter (Safaiyan et al., 2016), where CD11c$^{+}$
360 microglia were characteristically observed in aged mice (Hart, Wyttenbach, Perry, &
361 Teeling, 2012). Of note, the aging-induced expansion of microglia in the corpus
362 callosum was suppressed in Trem2 KO mice (Poliani et al., 2015). Furthermore, an *in*
363 *vitro* study suggested that SIRPα on microglia inhibited the phagocytosis of myelin
364 membrane fractions through interactions with CD47 on myelin (Gitik et al., 2011). Thus,
365 our present data support the model whereby the lack of CD47-SIRPα signal upregulates
366 the phagocytosis of microglia, which become hypersensitive to the homeostatic

367 destruction of myelin structures during the normal turnover process, and thereby
368 triggers the induction of CD11c$^+$ microglia without damage.
369 Transcriptome analyses showed that the expression of TNF-α, a proinflammatory
370 cytokine, was increased 2-3-fold in the brain monocytes isolated from CD47 KO mice.
371 In addition, pathway analysis showed other genes related to TNF and NF-κ B signalling
372 pathway, including RelA and IKKB (*Ikbkb*), were specifically increased in the mutant
373 brain cells. Thus, it is likely that proinflammatory TNF axis is strengthened in microglia
374 by the lack of CD47-SIRPα signal. In contrast, Wnt signal pathway, which contributes
375 to the proinflammatory transformation of microglia (Halleskog et al., 2011), was
376 attenuated in the CD47 KO brain cells. The transcriptome analysis also showed that
377 expression of TGF-β, an anti-inflammatory cytokine, and brain-derived neurotrophic
378 factor (BDNF), a neuroprotective factor, were increased in the CD47 KO brain cells.
379 Thus, it is not clear whether CD11c$^+$ microglia in the mutant mice have pro or
380 anti-inflammatory roles.
381 The expression of genes characteristic during the recovery phase from
382 demyelination (Holtman et al., 2015; Olah et al., 2012; Poliani et al., 2015), such as
383 *ItgaX*, *Igf1*, *Lpl*, *Apoc1*, *Ch25h*, *Mmp12*, *Spp1*, and *Cst7* were increased in both of the
384 white matter and the brain cells of CD47 KO mice, suggesting their upregulation in the
385 white matter CD11c$^+$ microglia, and also suggesting the potential of the CD11c$^+$
386 microglia to promote white matter tissue repair. Consistently, both demyelination and
387 microgliosis after 5 wks of Cpz feeding were significantly reduced in SIRPα cKO mice.
388 Although the direct involvement of CD11c$^+$ microglia on the reduction of demyelination
389 damage in the mutant mice is not yet clear, CD11c$^+$ microglia are likely to have a
390 protective effect against Cpz-induced demyelination. IGF-1 and Spp1 were increased in
391 the white matter and brain mononuclear cells in CD47 KO mice. These factors derived
392 from microglia and support the proliferation and differentiation of oligodendrocytes and
393 myelination (Olah et al., 2012; Selvaraju et al., 2004; Zeger et al., 2007).

394 CD11c$^+$ microglial in neonatal brains are reported as the major source of IGF-1 and to
395 support primary myelination (Wlodarczyk et al., 2017). CD11c$^+$ microglia in our mutant
396 mice could facilitate white matter repair through the function of these factors. At early
397 stages of Cpz treatment (3 wks feeding with Cpz), microgliosis was significantly more
398 severe in SIRPα cKO mice compared with control mice, suggesting a faster response of
399 SIRPα-deficient microglia to oligodendrocyte damage. Although Cpz feeding induced
400 CD11c$^+$ microglia in both control and SIRPα cKO mice, the preceding existence of
401 CD11c$^+$ microglia in SIRPα cKO mice may enable these cells to respond earlier to the
402 damage and accelerate tissue repair by their protective effect.
403 The loss and recovery of Olig2$^+$ cells were comparable between control and
404 SIRPα cKO mice during de- and re-myelination. Cell death and restorative proliferation
405 of the oligodendrocyte linage thus seems to occur in both groups to a similar extent. The
406 alleviated demyelination in SIRPα cKO mice may be explained by the faster
407 differentiation and/or maturation of oligodendrocytes compared with control mice,
408 resulting in accelerated remyelination in the cKO mice. Another possibility is that both
409 the cell death and restorative proliferation of oligodendrocytes were suppressed in
410 SIRPα cKO mice, resulting in reduced damage compared with control mice. In this case,
411 the total number of Olig2$^+$ cells, the summation of surviving and proliferating Olig2$^+$
412 cells, in SIRPα cKO would be comparable to control mice, in which both the loss and
413 restoration of Olig2$^+$ cells were much greater than in cKO mice, with greater
414 demyelination damage.
415 Our data suggest a supportive role for CD11c$^+$ microglia in tissue repair.
416 Consistently, the suppression of the emergence of CD11c$^+$ microglia by the genetic
417 ablation of Trem2 was concurrent with exacerbated neuronal damage in demyelination
418 model mice or neuronal death and amyloid deposition in AD model mice (Poliani et al.,
419 2015; Wang et al., 2015). The emergence of CD11c$^+$ microglia in aged brain might be
420 an adaptive reaction to cope with tissue damage caused by aging. It is also notable that

421 gene sets increased in the white matter of CD47 KO mice (i.e. *ItgaX, lpl, Cst7, Clec7a,*
422 *Trem2*, and *Tyrobp*) were similar to those increased in DAM (disease-associated
423 microglia), a potential protective microglia subtype associated with neurodegeneration
424 such as AD (Keren-Shaul et al., 2017). CD47-SIRPα interactions may be a key
425 mechanism for the induction of protective microglia such as DAM.

426 The reduction of demyelination in Cpz-treated SIRPα KO mice is in contrast to
427 persistent demyelination after Cpz treatment in Trem2 KO mice (Poliani et al., 2015). In
428 addition, the enhanced expression of *ItgaX*, *Igf1*, *Lpl*, *Ch25h*, and *Apoc1* in CD47 KO
429 mice was markedly in contrast to that in Trem2 KO mice, in which the upregulation of
430 these genes during demyelination in control mice were markedly suppressed (Poliani et
431 al., 2015). The signalling mechanisms of SIRPα and Trem2 are contrasting. SIRPα
432 activates tyrosine phosphatase Shp1/2, which binds to a phosphorylated ITIM in the
433 cytoplasmic region of SIRPα, while Trem2 activates tyrosine kinase Syk, which binds
434 to phosphorylated ITAM (immunoreceptor tyrosine-based activation motif) in the
435 cytoplasmic part of DAP12, a membrane protein forming a receptor complex with
436 Trem2 (Paradowska-Gorycka & Jurkowska, 2013). SIRPα and Trem2 may reciprocally
437 control microglia phagocytosis through the function of tyrosine phosphatase and kinase,
438 respectively. Further analysis of the interaction between CD47-SIRPα signalling and
439 Trem2-DAP12 signalling may be important to understand microglial activation and
440 phagocytosis and to identify new therapeutic strategies to promote tissue repair in the
441 damaged brain.

442 **Experimental Procedures**

443 **Animals**

444 SIRPα$^{-/-}$ (SIRPα KO), CD47$^{-/-}$ (CD47 KO), SIRPα$^{flox/flox}$, and Cx3cr1-CreER$^{T2}$ Tg
445 mice were generated as described (Oldenborg et al., 2000; Washio et al., 2015; Yona et
446 al., 2013). CD11c-Cre Tg mice [B6.Cg-Tg(Itgax-Cre)1-1Reiz/J, #008068] (Caton,
447 Smith-Raska, & Reizis, 2007) and CD11c-EYFP transgenic mice
448 [B6.Cg-Tg(Itgax-Venus)1Mnz/J, #008829] (Lindquist et al., 2004) were obtained from
449 Jackson Laboratory (Bar Harbor, ME). SIRPα KO mice were crossed with
450 CD11c-EYFP Tg mice to generate SIRPα$^{-/+}$:CD11c-EYFP Tg mice. These mice were
451 crossed with heterozygous SIRPα$^{-/+}$ mice, and the resulting homozygous SIRPα WT
452 and KO mice harbouring the CD11c-EYFP transgene were analysed. To obtain SIRPα
453 cKO mice, homozygous SIRPα-floxed mice harbouring the CD11c-Cre or
454 Cx3cr1-CreER$^{T2}$ transgene were crossed with homozygous floxed mice, and the
455 resulting SIRPα cKO (SIRPα$^{flox/flox}$:Cx3cr1-CreER$^{T2}$, SIRPα$^{flox/flox}$:CD11c-Cre) mice
456 were analysed. Littermates carrying homozygous SIRPα-flox alleles but lacking Cre
457 recombinase were used as controls. To induce Cre-dependent recombination,
458 Cx3cr1-CreER$^{T2}$ mice were treated with tamoxifen (TAM) (Toronto Research
459 Chemicals Inc., Ontario, Canada) at 8 wks of age. TAM was dissolved in ethanol and
460 then diluted 7 times with corn oil (Wako, Osaka, Japan) to make a 10 mg/ml solution,
461 and 200 μL (2 mg) of this solution was injected subcutaneously once every 48 h for 5
462 consecutive days (total of 3 times). TAM-treated mice were analysed more than 8
463 wks after the treatment. All mice were bred and maintained at the Bioresource Center
464 of Gunma University Graduate School of Medicine under specific pathogen–free
465 conditions. Mice were housed in an air-conditioned room with a 12-h-light, 12-h-dark
466 cycle. All animal experiments were approved by the Animal Care and Experimentation
467 Committee of Gunma University (approval no. 13-009).

468 **Primary antibodies and reagents**

469 Rabbit polyclonal antibodies (pAbs) to Iba1 were obtained from Wako (Osaka, Japan).
470 Biotin-conjugated Armenian Hamster monoclonal antibody (mAb) to mouse CD11c
471 (clone HL3), PerCP-Cy5.5 conjugated rat mAb to CD45 (30-F11), FITC-conjugated rat
472 mAb to mouse CD11b (clone M1/70), rat mAb to mouse CD16/CD32 (clone 2.4G2),
473 and streptavidin-conjugated allophycocyanin (APC) were from BD Pharmingen (San
474 Diego, CA). PE conjugated rat mAb to mouse CD172a (SIRPα) (clone P84) was from
475 eBioscience (San Diego, CA). PE conjugated and unconjugated rat mAbs to CD68
476 (clone FA-11) and PE conjugated rat mAb to mouse CD14 (clone Sa14-2) were from
477 BioLegend (San Diego, CA). PE conjugated recombinant antibody (Ab) to Dectin-1
478 (REA154) and PE conjugated recombinant Ab to CD47 (REA170) were from Miltenyi
479 Biotec (Bergisch Gladbach, Germany). 4',6-Diamidino-2-phenylindole (DAPI) was
480 obtained from Nacalai Tesque (Kyoto, Japan). Rat mAb to myelin basic protein (MBP)
481 (clone 12) was from Merck Millipore (Billerica, MA). Rabbit pAb to Olig2 (18953) was
482 from Immuno-Biological Laboratories (Minneapolis, MN).

483 **Histological analysis**

484 For immunohistochemistry, mice were anesthetised by the inhalation of isoflurane
485 (Pfizer, New York, NY) and an intraperitoneal injection of pentobarbital (Nembutal 100
486 mg/kg; Dynabot, Tokyo, Japan), and then perfused transcardially with fixation buffer
487 [4% paraformaldehyde in 0.1 M phosphate buffer (pH 7.4)]. Brain or spinal cord was
488 dissected and fixed in the fixation buffer overnight at 4°C, then transferred to 30%
489 sucrose in 0.1 M phosphate buffer (pH 7.4) for cryoprotection, embedded in OCT
490 compound (Sakura Fine Technical, Tokyo, Japan), and rapidly frozen in liquid nitrogen.
491 Frozen sections with a thickness of 10 or 20 μm were prepared with a cryostat, mounted
492 on glass slides, air dried, and washed with phosphate buffered saline (PBS). Otherwise,
493 free floating sections were washed with PBS. All sections were then incubated for 30
494 min at room temperature in Tyramide Signal Amplification (TSA) blocking solution
495 (Perkin Elmer, Norwalk, CT) and stained overnight at 8°C with primary antibodies

496 diluted in primary antibody dilution buffer (PBS supplemented with 2.5% BSA and
497 0.3% Triton X-100). Sections were then washed with PBS and exposed to the
498 corresponding secondary antibodies conjugated with the fluorescent dyes Cy3 (Jackson
499 Immuno Research Laboratories, West Grove, PA) or Alexa Fluor 488 (Invitrogen,
500 Carlsbad, CA) in secondary antibody dilution buffer (PBS supplemented with 1% BSA
501 and 0.3% Triton X-100). Nuclei were also stained with DAPI. The detection of CD11c
502 with biotin conjugated primary antibody (HL3) was achieved by using a TSA Biotin
503 System kit (Perkin Elmer) and streptavidin-conjugated Alexa Fluor 488 (Invitrogen)
504 according to the manufacturer's protocol. Free floating sections were mounted on glass
505 slides after staining. All sections were mounted with mounting media [0.1 M Tris-HCl
506 buffer (pH9) containing 5% 1,4-diazabicylo [2.2.2]-octane (DABCO), 20% polyvinyl
507 alcohol (PVA), 10% glycerol] and covered with a cover glass. Fluorescence images
508 were acquired with a fluorescence microscope BZ-X710 (Keyence, Osaka, Japan) or
509 DM RXA (Leica, Wetzlar, Germany) equipped with a cooled CCD camera (Cool SNAP
510 HQ; Roper Scientific, Trenton, NJ). Acquired digital images were analysed by ImageJ
511 software (Schneider, Rasband, & Eliceiri, 2012).
512 For myelin staining, frozen brain sections were mounted on a glass slide first, and
513 then stained with a Black-Gold II myelin staining kit (Merck Millipore) according to the
514 manufacturer's protocol. Images were acquired with a light microscope DM IRBE
515 (Leica) equipped with a cooled CCD camera (Penguin 600CL; Pixera Corp., Santa
516 Clara, CA).
517 **Preparation of microglia and flow cytometry**
518 Mononuclear cells including microglia were isolated by the method described by Sierra
519 *et al*. (Sierra, Gottfried-Blackmore, McEwen, & Bulloch, 2007) with a minor
520 modification. Briefly, brain or spinal cord was dissected from genotype- and
521 age-matched male mice euthanised by cervical dislocation after deep anaesthesia. Spinal
522 cords isolated from 1–3 mice were mixed and treated together. Tissues were rinsed in

523 ice-cold Hank's Balanced Salt Solution (HBSS; Gibco, Grand Island, NY) and then
524 homogenised in HBSS containing collagenase type 2 (37.5 U/ml; Worthington) and
525 DNase I (45 U/ml; Sigma). Homogenates were then incubated at 37°C for 30 min,
526 gently triturated with a Pasteur pipette, and incubated at 37°C for 10 min. Undigested
527 material was removed by filtration through a 70-μm cell strainer (BD Biosciences), and
528 the remaining cells were centrifuged at 1,100 ×*g* for 5 min at 18°C. Collected cells were
529 then suspended in 8 ml of 1×HBSS containing 70% Percoll (GE Healthcare Life
530 Science, Uppsala, Sweden), and then 4–5 ml of each was placed into a 15 ml tube. Cell
531 suspensions were then overlaid consecutively with 4 ml HBSS containing 37% Percoll
532 and 1 ml PBS. The resulting gradient was centrifuged at 200 ×*g* for 40 min at 18°C,
533 after which cells at the interface of the bottom 2 layers (70%/37%) were collected,
534 washed twice with HBSS, and subjected to flow cytometric analysis.
535 For flow cytometry analysis, cells were first incubated with a mAb specific
536 for mouse CD16/CD32 to prevent nonspecific binding of labelled mAbs against FcγR
537 and were then labelled with specific mAbs conjugated with PE, FITC, PerCP-Cy™5.5,
538 or biotin. For the staining of CD11c, a biotin-conjugated mAb against mouse CD11c
539 was detected with streptavidin-conjugated APC. Labelled cells were analysed by flow
540 cytometry using a BD FACS Canto II flow cytometer (BD Biosciences, San Jose, CA).
541 Cells were first gated on their forward (FSC) and side (SSC) scatter properties to
542 discriminate putative monocytes from other events, and then were gated on CD45 and
543 CD11b. The $CD11b^{+}/CD45^{dim/lo}$ fraction obtained was analysed as microglia. All data
544 were analysed with FlowJo 8.8.4 software (Tree Star Inc., Ashland, OR).
545 **Quantitative PCR analysis**
546 Total RNA was extracted from the whole brain, spinal cord, or dissected optic nerve
547 and optic tract with the use of Sepasol RNA I (Nacalai Tesque) and an RNeasy Mini kit
548 (Qiagen, Hilden, Germany). First-strand cDNA was synthesised from total RNA with
549 the use of a QuantiTect Reverse Transcription kit (Qiagen), and cDNA fragments of

550 interest were amplified by real-time PCR in 96-well plates (Roche Diagnostics,
551 Mannheim, Germany) with the use of a QuantiTect SYBR Green PCR kit (Qiagen) or
552 FastStart SYBR Green Master (Roche Diagnostics, Mannheim, Germany) and
553 LightCycler 480 or 96 Real-Time PCR System (Roche Diagnostics). The amplification
554 results were analysed with the use of LightCycler software and were then normalised on
555 the basis of the *Gapdh* mRNA level in each sample. Primer sequences (forward and
556 reverse, respectively) were as follows: *Tnfa*,
557 5'-CCCTCACACACTCAGATCATCTTCT-3' and
558 5'-GCTACGACGTGGGCTACAG-3'; *Il1b*,
559 5'-CAACCAACAAGTGATATTCTCCATG-3' and
560 5'-GATCCACACTCTCCAGCTGCA-3'; *Il6*,
561 5'-TAGTCCTTCCTACCCCAATTTCC-3' and
562 5'-TTGGTCCTTAGCCACTCCTTC-3'; *Il10*, 5'-AGGCGCTGTCATCGATTTCT-3'
563 and 5'-ATGGCCTTGTAGACACCTTGG-3'; *Tgfb*,
564 5'- ACCATGCCAACTTCTGTCTG-3' and 5'-CGGGTTGTGTTGGTTGTAGA-3';
565 *ItgaX*, 5'-AGCTGTGTGGACAGTGATGG-3' and
566 5'-TGCATGTGAGTCAGGAGGTC-3'; *Igf1*, 5'-TACTTCAACAAGCCCACAGGC-3'
567 and 5'-ATAGAGCGGGCTGCTTTTGT-3'; *Trem2*,
568 5'-CTTCCTGAAGAAGCGGAATG -3' and 5'-AGAGTGATGGTGACGGTTCC-3';
569 *Ccl3*, 5'-CAGCCAGGTGTCATTTTCCT-3' and 5'-CTGCCTCCAAGACTCTCAGG
570 -3'; and *Gapdh*, 5'-TCCCACTCTTCCACCTTCGA-3' and
571 5'-GTCCACCACCCTGTTGCTGTA-3'.

572 **Microarray analysis**

573 Total RNAs were prepared from the white matter (optic nerve and optic tract) or brain
574 mononuclear cells of WT or CD47 KO mice as described above. For the white matter,
575 RNAs from five (WT; 13-15 wks of age) and four (KO; 12-15 wks of age)
576 genotype-matched different male animals were pooled and subjected to the analysis. For

577 the brain mononuclear cells, RNAs from seven (WT; 10-15 wks of age) and six (KO;
578 12-16 wks of age) male animals were pooled and analysed. Microarray analyses were
579 performed by the Dragon Genomics Center of Takara Bio (Otsu, Japan). The quality of
580 RNA samples was confirmed by an Agilent 2100 Bioanalyzer (Agilent Technologies,
581 Palo Alto, CA). Biotinylated complementary RNA (cRNA) was synthesized using the
582 GeneChip 3'IVT Express Kit (Affymetrix, Santa Clara, CA) from 250 ng of total RNA
583 prepared from the white matter, or using the Ovation Pico WTA systemV2 (NuGEN,
584 San Carlos, CA) and Encore Biotin Module (NuGEN) from 20 ng of total RNA
585 prepared from the brain mononuclear cells. Following fragmentation, 10 μg of cRNA
586 was hybridised for 16 h at 45°C on the GeneChip Mouse Genome 430 2.0 Array
587 (Affymetrix) with the use of Hybridization, Wash and Stain Kit according to the
588 GeneChip 3'IVT Express Kit User Manual (Affymetrix). GeneChips were then scanned
589 by a GeneChip Scanner 3000 7G (Affymetrix) under the control of Affymetrix
590 GeneChip Command Console Software (Affymetrix). Obtained data were processed
591 using the Expression Console Software (Affymetrix).

592 **Transmission Electron Microscopy (TEM)**

593 Sample preparation for TEM analysis was carried out as described previously (Wilke et
594 al., 2013) with minor modifications. Mice were anesthetised as described above and
595 were then perfused transcardially with 1.6% PFA and 3% glutaraldehyde in 0.1 M
596 phosphate buffer (pH 7.4). Brain tissues were removed and fixed with 4% PFA in 0.1 M
597 phosphate buffer overnight at 4°C. Brains were coronally sectioned into slices of
598 100-μm thickness, and these slices were incubated with a fixative containing 2%
599 reduced $OsO_4$ and 1.5% potassium ferrocyanide in 0.1 M sodium cacodylate buffer (pH
600 7.4) for 1 h on ice, with 1% thiocarbohydrazide solution for 20 min at room temperature
601 and then with 2% OsO4 solution for 30 min. Sections were incubated in 1% uranyl
602 acetate overnight at 4°C, incubated with Walton's lead aspartate solution for 75 min at
603 60°C, dehydrated by sequential treatment for 10 min in each of 50, 70, 80, 90, 95, and

604 100% ethanol, and then placed in a second solution of 100% ethanol. The sections were
605 incubated with propylene oxide twice, with a 1:1 mixture of propylene oxide/Durcupan
606 resin (Durcupan ACM, Fluka, Buchs, Switzerland) for 10 min, with Durcupan resin
607 twice for 10 min each and then cured on a slide glass at 60°C for 2 days. The cured
608 resins containing the anterior commissure were trimmed out from the flat resins under a
609 stereo microscope and re-embedded into resin blocks for ultrathin sectioning. Ultrathin
610 sections were prepared at a 50-nm thickness using an ultramicrotome (Ultracut-T,
611 Leica) and collected onto single slot copper grids. The samples were examined at ×2500
612 magnification by a transmission electron microscope (H-7650, Hitachi, Tokyo, Japan)
613 and digital electron micrographs were captured. The frequency of myelinated axons
614 among all axons in the anterior commissure and g-ratios of myelinated axons, the ratio
615 of circumference of axon over myelin, were determined by the use of iTEM software
616 (Olympus SIS, Münster, Germany).

617 **Cuprizone model of demyelination**

618 Control (SIRPα$^{fl/fl}$:—) or SIRPα cKO (SIRPα$^{fl/fl}$:Cx3cr1CreER$^{T2}$) mice were fed a 0.2%
619 (*w/w*) cuprizone [bis(cyclohexanone)oxaldihydrazone, Sigma] (Cpz) diet. Mice were
620 sacrificed and their brains were processed for immunohistochemical analysis after 3 or
621 5 wks of Cpz treatment. Other groups of mice were returned to a normal diet after 5 wks
622 of Cpz treatment and allowed to recover for 2 wks prior to immunohistochemical
623 analysis. Mice fed a normal diet without Cpz for 7 wks were analysed as controls.
624 Frozen brain coronal sections with a thickness of 20 μm were prepared and stained with
625 specific antibodies for MBP (Myelin Basic Protein), Iba1, CD11c, and Olig2. Coronal
626 slices from each mouse at approximate levels −1.9 to −2.0 mm from the bregma
627 (Paxinos & Franklin, 1997) were analysed by fluorescence microscopy. Acquired
628 digital images were analysed by ImageJ software (Schneider et al., 2012) to quantify the
629 area of demyelination or microgliosis and the number of Olig2$^{+}$ cells.

630 **Statistical analysis**

631 Data are presented as the means ± SEM and were analysed by the Student's *t*-test. A *P*
632 value < 0.05 was considered statistically significant.

633 **Data availability**

634 The microarray data have been deposited to the Gene Expression Omnibus database
635 (https://www.ncbi.nlm.nih.gov/geo/) (accession numbers: GSE118804 and GSE118805
636 for the white matter and the brain mononuclear cells, respectively).

**Acknowledgments**

We thank E. Urano and T. Maegawa for technical assistance. This work was supported by a Grant-in-Aid for Scientific Research on Innovative Areas ("Brain Environment"), a Grant-in-Aid for Scientific Research (C), and a Grant-in-Aid for Challenging Exploratory Research from the Ministry of Education, Culture, Sports, Science and Technology of Japan, and a grant from Takeda Science Foundation of Japan.

**Author Contributions**

H. O. conceived the research and wrote paper; H.O. and M. S.-H. designed and conducted the experiments, and analysed the data; T. I., R. E., and Y. F. performed electron microscopic analysis; T. N., R. T., H. N., A. Horikoshi, M. A., Y. H., W. S., A. Hirose, K. K., and A. S. conducted the experiments and analysed data. T. K., Y. M., Y. S., M. N., K. S., P.-A. O., S. J. and T. M. contributed to the experimental resources and wrote the paper. All authors reviewed the manuscript.

**Declaration of Interests**

The authors declare no competing interests.

656 **References**


657 Acevedo, G., Padala, N. K., Ni, L., & Jonakait, G. M. (2013). Astrocytes inhibit
658 microglial surface expression of dendritic cell-related co-stimulatory molecules
659 through a contact-mediated process. *J Neurochem, 125*(4), 575-587.
660 doi:10.1111/jnc.12221

661 Barclay, A. N., & Hatherley, D. (2008). The counterbalance theory for evolution and
662 function of paired receptors. *Immunity, 29*(5), 675-678.
663 doi:10.1016/j.immuni.2008.10.004

664 Baumann, N., & Pham-Dinh, D. (2001). Biology of oligodendrocyte and myelin in the
665 mammalian central nervous system. *Physiol Rev, 81*(2), 871-927.
666 doi:10.1152/physrev.2001.81.2.871

667 Bulloch, K., Miller, M. M., Gal-Toth, J., Milner, T. A., Gottfried-Blackmore, A.,
668 Waters, E. M., . . . McEwen, B. S. (2008). CD11c/EYFP transgene illuminates a
669 discrete network of dendritic cells within the embryonic, neonatal, adult, and
670 injured mouse brain. *J Comp Neurol, 508*(5), 687-710. doi:10.1002/cne.21668

671 Cantoni, C., Bollman, B., Licastro, D., Xie, M., Mikesell, R., Schmidt, R., . . . Piccio, L.
672 (2015). TREM2 regulates microglial cell activation in response to demyelination
673 in vivo. *Acta Neuropathol, 129*(3), 429-447. doi:10.1007/s00401-015-1388-1

674 Caton, M. L., Smith-Raska, M. R., & Reizis, B. (2007). Notch-RBP-J signaling controls
675 the homeostasis of $CD8^-$ dendritic cells in the spleen. *J Exp Med, 204*(7),
676 1653-1664. doi:10.1084/jem.20062648

677 Chao, M. P., Tang, C., Pachynski, R. K., Chin, R., Majeti, R., & Weissman, I. L. (2011).
678 Extranodal dissemination of non-Hodgkin lymphoma requires CD47 and is
679 inhibited by anti-CD47 antibody therapy. *Blood, 118*(18), 4890-4901.
680 doi:10.1182/blood-2011-02-338020

681 Chiu, I. M., Morimoto, E. T., Goodarzi, H., Liao, J. T., O'Keeffe, S., Phatnani, H. P., . . .
682 Maniatis, T. (2013). A neurodegeneration-specific gene-expression signature of

683 acutely isolated microglia from an amyotrophic lateral sclerosis mouse model.
684 *Cell Rep, 4*(2), 385-401. doi:10.1016/j.celrep.2013.06.018
685 Gitik, M., Liraz-Zaltsman, S., Oldenborg, P. A., Reichert, F., & Rotshenker, S. (2011).
686 Myelin down-regulates myelin phagocytosis by microglia and macrophages
687 through interactions between CD47 on myelin and SIRPα (signal regulatory
688 protein-α) on phagocytes. *J Neuroinflammation, 8*, 24.
689 doi:10.1186/1742-2094-8-24
690 Goldmann, T., Wieghofer, P., Müller, P. F., Wolf, Y., Varol, D., Yona, S., . . . Prinz, M.
691 (2013). A new type of microglia gene targeting shows TAK1 to be pivotal in
692 CNS autoimmune inflammation. *Nat Neurosci, 16*(11), 1618-1626.
693 doi:10.1038/nn.3531
694 Gudi, V., Gingele, S., Skripuletz, T., & Stangel, M. (2014). Glial response during
695 cuprizone-induced de- and remyelination in the CNS: lessons learned. *Front*
696 *Cell Neurosci, 8*, 73. doi:10.3389/fncel.2014.00073
697 Halleskog, C., Mulder, J., Dahlström, J., Mackie, K., Hortobágyi, T., Tanila, H., . . .
698 Schulte, G. (2011). WNT signaling in activated microglia is proinflammatory.
699 *Glia, 59*(1), 119-131. doi:10.1002/glia.21081
700 Hart, A. D., Wyttenbach, A., Perry, V. H., & Teeling, J. L. (2012). Age related changes
701 in microglial phenotype vary between CNS regions: grey versus white matter
702 differences. *Brain Behav Immun, 26*(5), 754-765. doi:10.1016/j.bbi.2011.11.006
703 Holtman, I. R., Raj, D. D., Miller, J. A., Schaafsma, W., Yin, Z., Brouwer, N., . . .
704 Eggen, B. J. (2015). Induction of a common microglia gene expression signature
705 by aging and neurodegenerative conditions: a co-expression meta-analysis. *Acta*
706 *Neuropathol Commun, 3*, 31. doi:10.1186/s40478-015-0203-5
707 Huang, D. W., Sherman, B. T., & Lempicki, R. A. (2009a). Bioinformatics enrichment
708 tools: paths toward the comprehensive functional analysis of large gene lists.
709 *Nucleic Acids Res, 37*(1), 1-13. doi:10.1093/nar/gkn923

710 Huang, D. W., Sherman, B. T., & Lempicki, R. A. (2009b). Systematic and integrative
711 analysis of large gene lists using DAVID bioinformatics resources. *Nat Protoc,*
712 *4*(1), 44-57. doi:10.1038/nprot.2008.211
713 Ishikawa-Sekigami, T., Kaneko, Y., Okazawa, H., Tomizawa, T., Okajo, J., Saito,
714 Y., . . . Nojima, Y. (2006). SHPS-1 promotes the survival of circulating
715 erythrocytes through inhibition of phagocytosis by splenic macrophages. *Blood,*
716 *107*(1), 341-348. doi:10.1182/blood-2005-05-1896
717 Jaiswal, S., Jamieson, C. H., Pang, W. W., Park, C. Y., Chao, M. P., Majeti, R., . . .
718 Weissman, I. L. (2009). CD47 is upregulated on circulating hematopoietic stem
719 cells and leukemia cells to avoid phagocytosis. *Cell, 138*(2), 271-285.
720 doi:10.1016/j.cell.2009.05.046
721 Kamphuis, W., Kooijman, L., Schetters, S., Orre, M., & Hol, E. M. (2016).
722 Transcriptional profiling of CD11c-positive microglia accumulating around
723 amyloid plaques in a mouse model for Alzheimer's disease. *Biochim Biophys*
724 *Acta, 1862*(10), 1847-1860. doi:10.1016/j.bbadis.2016.07.007
725 Kaunzner, U. W., Miller, M. M., Gottfried-Blackmore, A., Gal-Toth, J., Felger, J. C.,
726 McEwen, B. S., & Bulloch, K. (2012). Accumulation of resident and peripheral
727 dendritic cells in the aging CNS. *Neurobiol Aging, 33*(4), 681-693.e681.
728 doi:10.1016/j.neurobiolaging.2010.06.007
729 Keren-Shaul, H., Spinrad, A., Weiner, A., Matcovitch-Natan, O., Dvir-Szternfeld, R.,
730 Ulland, T. K., . . . Amit, I. (2017). A unique microglia type associated with
731 restricting development of Alzheimer's disease. *Cell, 169*(7), 1276-1290.e1217.
732 doi:10.1016/j.cell.2017.05.018
733 Kettenmann, H., Hanisch, U. K., Noda, M., & Verkhratsky, A. (2011). Physiology of
734 microglia. *Physiol Rev, 91*(2), 461-553. doi:10.1152/physrev.00011.2010

735 Kojima, Y., Volkmer, J. P., McKenna, K., Civelek, M., Lusis, A. J., Miller, C. L., . . .
736 Leeper, N. J. (2016). CD47-blocking antibodies restore phagocytosis and
737 prevent atherosclerosis. *Nature, 536*(7614), 86-90. doi:10.1038/nature18935
738 Kusakari, S., Ohnishi, H., Jin, F. J., Kaneko, Y., Murata, T., Murata, Y., . . . Matozaki,
739 T. (2008). Trans-endocytosis of CD47 and SHPS-1 and its role in regulation of
740 the CD47-SHPS-1 system. *J Cell Sci, 121*(Pt 8), 1213-1223.
741 doi:10.1242/jcs.025015
742 Lampron, A., Larochelle, A., Laflamme, N., Préfontaine, P., Plante, M. M., Sánchez, M.
743 G., . . . Rivest, S. (2015). Inefficient clearance of myelin debris by microglia
744 impairs remyelinating processes. *J Exp Med, 212*(4), 481-495.
745 doi:10.1084/jem.20141656
746 Lindquist, R. L., Shakhar, G., Dudziak, D., Wardemann, H., Eisenreich, T., Dustin, M.
747 L., & Nussenzweig, M. C. (2004). Visualizing dendritic cell networks in vivo.
748 *Nat Immunol, 5*(12), 1243-1250. doi:10.1038/ni1139
749 Matozaki, T., Murata, Y., Okazawa, H., & Ohnishi, H. (2009). Functions and molecular
750 mechanisms of the CD47-SIRPα signalling pathway. *Trends Cell Biol, 19*(2),
751 72-80. doi:10.1016/j.tcb.2008.12.001
752 Matsuo, A., Akiguchi, I., Lee, G. C., McGeer, E. G., McGeer, P. L., & Kimura, J.
753 (1998). Myelin degeneration in multiple system atrophy detected by unique
754 antibodies. *Am J Pathol, 153*(3), 735-744. doi:10.1016/S0002-9440(10)65617-9
755 Nishiyama, A., Komitova, M., Suzuki, R., & Zhu, X. (2009). Polydendrocytes (NG2
756 cells): multifunctional cells with lineage plasticity. *Nat Rev Neurosci, 10*(1),
757 9-22. doi:10.1038/nrn2495
758 Norden, D. M., & Godbout, J. P. (2013). Review: microglia of the aged brain: primed to
759 be activated and resistant to regulation. *Neuropathol Appl Neurobiol, 39*(1),
760 19-34. doi:10.1111/j.1365-2990.2012.01306.x

761 Norkute, A., Hieble, A., Braun, A., Johann, S., Clarner, T., Baumgartner, W., . . . Kipp,
762 M. (2009). Cuprizone treatment induces demyelination and astrocytosis in the
763 mouse hippocampus. *J Neurosci Res, 87*(6), 1343-1355. doi:10.1002/jnr.21946
764 Ohnishi, H., Murata, T., Kusakari, S., Hayashi, Y., Takao, K., Maruyama, T., . . .
765 Matozaki, T. (2010). Stress-evoked tyrosine phosphorylation of signal
766 regulatory protein α regulates behavioral immobility in the forced swim test. *J*
767 *Neurosci, 30*(31), 10472-10483. doi:10.1523/JNEUROSCI.0257-10.2010
768 Olah, M., Amor, S., Brouwer, N., Vinet, J., Eggen, B., Biber, K., & Boddeke, H. W.
769 (2012). Identification of a microglia phenotype supportive of remyelination.
770 *Glia, 60*(2), 306-321. doi:10.1002/glia.21266
771 Oldenborg, P. A., Zheleznyak, A., Fang, Y. F., Lagenaur, C. F., Gresham, H. D., &
772 Lindberg, F. P. (2000). Role of CD47 as a marker of self on red blood cells.
773 *Science, 288*(5473), 2051-2054.
774 Paradowska-Gorycka, A., & Jurkowska, M. (2013). Structure, expression pattern and
775 biological activity of molecular complex TREM-2/DAP12. *Hum Immunol, 74*(6),
776 730-737. doi:10.1016/j.humimm.2013.02.003
777 Paxinos, G., & Franklin, K. (1997). *The Mouse Brain in Stereotaxic Coordinates*. San
778 Diego: Academic Press.
779 Poliani, P. L., Wang, Y., Fontana, E., Robinette, M. L., Yamanishi, Y., Gilfillan, S., &
780 Colonna, M. (2015). TREM2 sustains microglial expansion during aging and
781 response to demyelination. *J Clin Invest, 125*(5), 2161-2170.
782 doi:10.1172/JCI77983
783 Ransohoff, R. M., & Cardona, A. E. (2010). The myeloid cells of the central nervous
784 system parenchyma. *Nature, 468*(7321), 253-262. doi:10.1038/nature09615
785 Remington, L. T., Babcock, A. A., Zehntner, S. P., & Owens, T. (2007). Microglial
786 recruitment, activation, and proliferation in response to primary demyelination.
787 *Am J Pathol, 170*(5), 1713-1724. doi:10.2353/ajpath.2007.060783

788 Safaiyan, S., Kannaiyan, N., Snaidero, N., Brioschi, S., Biber, K., Yona, S., . . . Simons,
789 M. (2016). Age-related myelin degradation burdens the clearance function of
790 microglia during aging. *Nat Neurosci, 19*(8), 995-998. doi:10.1038/nn.4325
791 Saijo, K., & Glass, C. K. (2011). Microglial cell origin and phenotypes in health and
792 disease. *Nat Rev Immunol, 11*(11), 775-787. doi:10.1038/nri3086
793 Schneider, C. A., Rasband, W. S., & Eliceiri, K. W. (2012). NIH Image to ImageJ: 25
794 years of image analysis. *Nat Methods, 9*(7), 671-675.
795 Selvaraju, R., Bernasconi, L., Losberger, C., Graber, P., Kadi, L., Avellana-Adalid,
796 V., . . . Boschert, U. (2004). Osteopontin is upregulated during in vivo
797 demyelination and remyelination and enhances myelin formation in vitro. *Mol*
798 *Cell Neurosci, 25*(4), 707-721. doi:10.1016/j.mcn.2003.12.014
799 Sierra, A., Gottfried-Blackmore, A. C., McEwen, B. S., & Bulloch, K. (2007).
800 Microglia derived from aging mice exhibit an altered inflammatory profile. *Glia,*
801 *55*(4), 412-424. doi:10.1002/glia.20468
802 Wang, Y., Cella, M., Mallinson, K., Ulrich, J. D., Young, K. L., Robinette, M. L., . . .
803 Colonna, M. (2015). TREM2 lipid sensing sustains the microglial response in an
804 Alzheimer's disease model. *Cell, 160*(6), 1061-1071.
805 doi:10.1016/j.cell.2015.01.049
806 Washio, K., Kotani, T., Saito, Y., Respatika, D., Murata, Y., Kaneko, Y., . . . Matozaki,
807 T. (2015). Dendritic cell SIRPα regulates homeostasis of dendritic cells in
808 lymphoid organs. *Genes Cells, 20*(6), 451-463. doi:10.1111/gtc.12238
809 Wilke, S. A., Antonios, J. K., Bushong, E. A., Badkoobehi, A., Malek, E., Hwang,
810 M., . . . Ghosh, A. (2013). Deconstructing complexity: serial block-face electron
811 microscopic analysis of the hippocampal mossy fiber synapse. *J Neurosci, 33*(2),
812 507-522. doi:10.1523/JNEUROSCI.1600-12.2013
813 Willingham, S. B., Volkmer, J. P., Gentles, A. J., Sahoo, D., Dalerba, P., Mitra, S.
814 S., . . . Weissman, I. L. (2012). The CD47-signal regulatory protein alpha

(SIRPa) interaction is a therapeutic target for human solid tumors. *Proc Natl Acad Sci U S A, 109*(17), 6662-6667. doi:10.1073/pnas.1121623109

Wlodarczyk, A., Holtman, I. R., Krueger, M., Yogev, N., Bruttger, J., Khorooshi, R., . . . Owens, T. (2017). A novel microglial subset plays a key role in myelinogenesis in developing brain. *EMBO J, 36*(22), 3292-3308. doi:10.15252/embj.201696056

Wolf, Y., Yona, S., Kim, K. W., & Jung, S. (2013). Microglia, seen from the CX3CR1 angle. *Front Cell Neurosci, 7*, 26. doi:10.3389/fncel.2013.00026

Yona, S., Kim, K. W., Wolf, Y., Mildner, A., Varol, D., Breker, M., . . . Jung, S. (2013). Fate mapping reveals origins and dynamics of monocytes and tissue macrophages under homeostasis. *Immunity, 38*(1), 79-91. doi:10.1016/j.immuni.2012.12.001

Zeger, M., Popken, G., Zhang, J., Xuan, S., Lu, Q. R., Schwab, M. H., . . . Ye, P. (2007). Insulin-like growth factor type 1 receptor signaling in the cells of oligodendrocyte lineage is required for normal in vivo oligodendrocyte development and myelination. *Glia, 55*(4), 400-411. doi:10.1002/glia.20469

831 **Figure legends**

832 **Figure 1. Activation of microglia in the brain white matter of SIRPα KO mice.** (**A**)
833 Immunofluorescence staining of coronal brain sections prepared from control (**WT**) or
834 SIRPα null mutant mice (**SIRPα KO**) with antibodies to Iba1 (***red***) and CD68 (***green***).
835 Merged images are shown. **fi**: fimbria. (**B**) Quantitative analysis of the number of Iba1$^+$
836 (***left panel***) and Iba1$^+$/CD68$^+$ (***right panel***) microglia in the fimbria of WT (**filled bars**)
837 and SIRPα KO mice (**open bars**) at 18–20 wks of age. Data are the means ± SEM ($n$ =
838 6 images from 3 mice for each genotype). $^{**}P < 0.01$ (Student's $t$-test). (**C, D**)
839 Immunofluorescence staining of coronal brain sections prepared from control
840 CD11c-EYFP Tg mice carrying a homozygous SIRPα WT allele (SIRPα
841 WT:CD11c-EYFP, ***left side***) or SIRPα null mutation (SIRPα KO:CD11c-EYFP, ***right***
842 ***side***) at 30–32 wks of age. Images in **C** are lower magnification images of the
843 immunoreactivity of Iba1 (***upper panels***) and fluorescence of EYFP in the same
844 sections (***lower panels***). Images were converted to grey scale and then inverted to
845 clarify the fluorescence signal. Images in **D** are higher magnification images of the
846 immunoreactivity of Iba1 (***red***) and fluorescence of EYFP (***green***) in grey (cerebrum
847 cortex; **ctx,** ***upper panels***) and white matter (external capsule; **ec,** ***lower panels***). **ctx**:
848 cerebrum cortex, **cc**: corpus callosum, **ec**: external capsule, **fi**: fimbria, **int**: internal
849 capsule. Data are representative of at least 3 independent animals. Scale bars: 100 μm
850 (**A**), 1 mm (**C**), and 50 μm (**D**).

851

852 **Figure 2. CD11c$^+$ microglia in the white matter of SIRPα KO mice.** (**A, B**) Coronal
853 sections prepared from brain (**A**) and spinal cord (**B**) of control (**WT**) or SIRPα null
854 mutant mice (**SIRPα KO**) at 18–20 wks of age with antibodies to Iba1 (***red***) and
855 CD11c (***green***). In **A**, merged images are shown. Schematic diagrams of brain sections
856 are shown on the left side. The boxed areas in **B** are shown at a higher magnification in
857 the lower panels. **ctx**: cerebrum cortex, **cc**: corpus callosum, **och**: optic chiasma. (**C, D**)

858 Coronal brain sections of control (**WT**) or SIRPα null mutant mice (**SIRPα KO**) at 29–
859 32 (**C**) or 10–11 (**D**) wks of age with antibodies to myelin basic protein (**MBP**) (***red***)
860 and CD11c (***green***) (**C**), or Black-Gold (**D**). **cc**: corpus callosum, **fi**: fimbria, **ac**:
861 anterior commissure. Data are representative of at least 3 independent animals. Scale
862 bars, 50 μm (**A, B *lower panels***), 1 mm (**B *upper panels***), 100 μm (**C**), and 200 μm (**D**).
863
864 **Figure 3. Flow cytometry analysis of microglia in SIRPα KO mice and WT aged**
865 **mice.** (**A**) Cells isolated from the spinal cord of control WT or SIRPα KO (**KO**) mice
866 at 14 wks of age were incubated with a PE-conjugated mAb to SIRPα, a PerCP-Cy5.5–
867 conjugated mAb to CD45, and an FITC-conjugated mAb to CD11b. The expressions of
868 CD11b and CD45 on monocyte cells or of SIRPα on $CD11b^{+}/CD45^{dim/lo}$ microglia was
869 analysed by flow cytometry. The percentage of $CD11b^{+}/CD45^{dim/lo}$ microglia among
870 putative monocytes is indicated on each plot (***left plots***). Expression profiles for SIRPα
871 on $CD11b^{+}/CD45^{dim/lo}$ microglia are shown in the right panel. (**B**) Cells prepared as in **A**
872 from WT or SIRPα KO mice at 14–21 wks of age were stained with antibodies to
873 CD45, CD11b, and CD11c, and analysed by flow cytometry. The percentage of
874 $CD11b^{+}/CD45^{dim/lo}/CD11c^{+}$ microglia among total $CD11b^{+}/CD45^{dim/lo}$ microglia is
875 indicated on each plot. Quantitative data are shown in the right panel. (**C**) Cells
876 prepared from SIRPα KO mice were stained for CD45, CD11b and CD11c, as well as
877 CD14, Dectin-1, or CD68. Plots were gated on $CD11b^{+}/CD45^{dim/lo}$ cells and CD14,
878 Dectin-1, or CD68 on CD11c-positive and –negative microglia were analysed.
879 Expression profiles for each molecule in $CD11b^{+}/CD45^{dim/lo}$ microglia are shown. (**D**)
880 Cells isolated from adult (18 wks of age) or aged (104 wks of age) mice were isolated
881 and analysed as in **A**. (**E**) Cells prepared as in **D** from adult (16–18 wks of age) or
882 aged (69–105 wks of age) mice were analysed as in **B**. Quantitative data are shown in
883 the right panel. (**F**) Cells prepared from aged mice were analysed as in **C**. Data in **B**
884 and **E** are the means ± SEM [$n$ = 3 (**B**) and 5 (**E**) independent experiments]. ***$P$ <

885 0.001 (Student's *t*-test). Other data are representative of at least 3–5 independent
886 experiments. Filled and open traces in (**A**), (**C, F**), and (**D**) indicate WT and SIRPα KO
887 mice, $CD11c^{-}$ and $CD11c^{+}$ cells, and adult and aged mice, respectively.
888
889 **Figure 3—figure supplement 1. Forward (FSC) and side (SSC) scatter distribution**
890 **of $CD11c^{+}$ microglia.** FSC/SSC distribution of WT (***upper panels***) and SIRPα KO
891 (***lower panels***) microglia were analyzed. $CD11c^{+}$ and $CD11c^{-}$ microglia in the left
892 panels (events in the solid and dotted rectangles, respectively) are presented on the
893 FSC/SSC plots in the right panels. Scatter plots in the left panels are identical to
894 those shown in **Figure 3B**. All data used in **Figure 3B** were analysed in the same way,
895 and representative results were shown.
896
897 **Figure 3—figure supplement 2. Expression of pro and anti-inflammatory cytokines**
898 **in the brain and spinal cord of SIRPα KO mice.** Whole brains and spinal cords were
899 dissected from WT or SIRPα KO mice at 13–20 wks of age for the isolation of total
900 RNA. The expressions of the indicated cytokines were then determined by quantitative
901 polymerase chain reaction (PCR) analysis. The amount of each mRNA was normalised
902 to that of glyceraldehyde-3-phosphate dehydrogenase (GAPDH) mRNA and is
903 presented relative to the mean value for control WT mice. Data are the means ± SEM (*n*
904 = 6 mice for each genotype). $*P < 0.05$ (Student's *t*-test).
905
906 **Figure 4. Activation of microglia in the brain white matter of CD47 KO mice.** (**A**)
907 Immunofluorescence staining of coronal brain sections prepared from control (**WT**) or
908 CD47 KO mice at 19 wks of age with antibodies to Iba1 (***red***) and CD11c (***green***).
909 Merged images are shown. The boxed areas in the upper panels are shown at higher
910 magnification in the lower panels. **fi**: fimbria. Scale bars: 100 μm (***upper panels***), 50
911 μm (***lower panels***). (**B**) Quantitative analysis of the number of $Iba1^{+}$ (***left panel***) and

912 Iba1$^{+}$/CD11c$^{+}$ (***right panel***) microglia in the fimbria of WT (**filled bars**) and CD47 KO
913 mice (**open bars**) at 13–27 wks of age. Data are the means ± SEM ($n$ = 3 images from 3
914 mice for each genotype). **$P$ < 0.01 (Student's $t$-test). (**C**) Cells were isolated from the
915 spinal cord of WT or CD47 KO mice at 14–16 wks of age. Expressions of CD47 or
916 SIRPα on CD11b$^{+}$/CD45$^{dim/lo}$ microglia were analysed by flow cytometry. Data are
917 representative of at least 3 independent experiments.
918
919 **Figure 5. Microarray transcriptome analyses of the white matter and the brain**
920 **mononuclear cells of CD47 KO mice.** (**A**, **B**) The results of Kyoto Encyclopedia of
921 Genes and Genomes (KEGG) pathway analysis with DAVID. Statistically significant
922 ($P$-value < 0.01) KEGG enrichment pathways of up- (**A**) or down- (**B**) regulated genes
923 in the white matter (optic nerve and optic tract) (***upper panels***) or in the brain
924 mononuclear cells (***lower panels***) of CD47 KO mice were shown. Enrichment score is
925 expressed as -Log ($p$-value). **ARVC:** Arrhythmogenic right ventricular cardiomyopathy,
926 **HCM:** Hypertrophic cardiomyopathy. (**C**) The expression changes of the selected genes
927 characteristics of microglia or of de- and re-myelination processes. For each probe set
928 on the microarray, the fold-change of gene expression in the CD47 KO mice compared
929 with WT mice was expressed as a log2 ratio. Open and grey bars show the comparison
930 in the white matter and the brain mononuclear cells, respectively. Probe set ID#:
931 Affymetrix probe set ID number.
932
933 **Figure 5—figure supplement 1. Quantitative PCR analyses of the white matter**
934 **RNA.** Total RNA samples from the optic chiasm and optic nerve of CD47 KO and WT
935 mice ($n$ = 4 and 6, respectively) were subjected to quantitative PCR analysis to
936 determine the expression of the indicated genes. The amount of each mRNA was
937 normalised to that of glyceraldehyde-3-phosphate dehydrogenase (GAPDH) mRNA and

938 presented relative to the mean value for control WT mice. Data are the means ± SEM.
939 $^{**}P < 0.01$ (Student's *t*-test).
940
941 **Figure 5—figure supplement 2. Genes commonly changed in both of the white**
942 **matter and the brain mononuclear cells.** The genes commonly changed more than
943 2-fold (|Log2 ratio| > 1) in both of the white matter and the brain mononuclear cells of
944 CD47 KO mice were listed. **probe set ID#:** Affymetrix probe set ID number for Mouse
945 430 2.0 Genome Arrays, **gene:** gene description, **symbol:** gene symbol, **accession:**
946 NCBI accession number, **Log2 ratio:** fold change expressed as Log2 (KO/WT).
947
948 **Figure 6. Phenotypes of microglia-specific SIRPα conditional knockout mice.** (**A**)
949 Cells isolated from the brains of control (**SIRPα$^{fl/fl}$:—**) or microglia-specific SIRPα
950 cKO (**SIRPα$^{fl/fl}$:Cx3cr1-CreER$^{T2}$**) mice at 11 wks of age were stained as in **Figure 3A**.
951 The percentage of CD11b$^{+}$/CD45$^{dim/lo}$/SIRPα$^{+}$ or /SIRPα$^{-}$ microglia among total
952 CD11b$^{+}$/CD45$^{dim/lo}$ microglia is indicated on each plot. Data are representative of at least
953 4 independent experiments. (**B**) Immunofluorescence staining of coronal brain sections
954 prepared from control (SIRPα$^{fl/fl}$) and SIRPα cKO mice at 22 wks of age with
955 antibodies to Iba1 (***red***) and CD11c (***green***). Merged images are shown. The boxed
956 areas in the upper panels are shown at higher magnification in the lower panels. **fi**:
957 fimbria. Scale bars: 200 μm (***upper panels***), 50 μm (***lower panels***). (**C**) Quantitative
958 analysis of the number of Iba1$^{+}$ (***left panel***) and Iba1$^{+}$/CD11c$^{+}$ (***right panel***) microglia in
959 the fimbria of control (SIRPα$^{fl/fl}$) (**filled bars**) and SIRPα cKO (**cKO**) mice (**open bars**)
960 at 22 wks of age. Data are the means ± SEM ($n$ = 4 images from 2 mice for each
961 genotype). $^{**}P < 0.01$ (Student's *t*-test). **N.D.**: not detected. (**D**) Electron microscopic
962 analysis of axon fibres in the anterior commissure of control (**SIRPα$^{fl/fl}$:—**) and
963 microglia-specific SIRPα cKO mice (**SIRPα$^{fl/fl}$:Cx3cr1-CreER$^{T2}$**) at 26–27 wks of age.
964 Scale bar: 2 μm. (**E**) Quantitative data of the myelination ratio (percentage of

965 myelinated axons in total number of axons) and g-ratio (a ratio of the inner axonal
966 diameter to the total outer diameter of myelinated axons) in the anterior commissure of
967 three control (#1–#3, ***filled bars***) and cKO mice (#4–#6, ***open bars***). The myelination
968 ratio and g-ratio were calculated from 9–10 images (109–465 axons/image) ($n$ = 9–10)
969 and 317–562 myelinated axons in 9–10 images ($n$ = 317–562), respectively, for each
970 mouse. Data are the means ± SEM.
971
972 **Figure 6—figure supplement 1. Immunohistochemical analysis of CD11c$^{+}$**
973 **cell-specific SIRPα conditional knockout mice.** Brain sections prepared from control
974 (**SIRPα$^{fl/fl}$:—**) and CD11c$^{+}$ cell-specific SIRPα cKO (**SIRPα$^{fl/fl}$:CD11c-Cre**) mice at
975 25 wks of age were immunostained as in **Figure 6B**. Merged images are shown. **fi**:
976 fimbria. Data are representative of at least 3 independent animals. Scale bar: 100 μm.
977
978 **Figure 7. Alleviation of cuprizone-induced demyelination in SIRPα cKO mice.** (**A**)
979 Control SIRPα$^{fl/fl}$ (**Ctrl**) or SIRPα cKO [SIRPα$^{fl/fl}$:Cx3cr1-CreER$^{T2}$ (**cKO**)] mice at 20–
980 25 wks of age were fed a 0.2% (*w/w*) cuprizone (**Cpz**) diet. After 3 or 5 wks of Cpz
981 feeding (**Cpz 3 wks**, **Cpz 5 wks**), brain samples were prepared. Other groups of mice
982 were returned to a normal diet after 5 wks of Cpz treatment and allowed to recover for 2
983 wks prior to the tissue analysis (**Rec 2 wks**). Mice fed a normal diet without Cpz for 7
984 wks were analysed as controls (**Basal**). Brain sections were subjected to
985 immunofluorescence staining with specific antibodies for MBP, CD11c, Iba1, and
986 Olig2. Arrowheads and arrows indicate typical demyelination (**MBP**) or microgliosis
987 (**Iba1**) in the corpus callosum (*arrowheads*) and hippocampal alveus (*arrows*).
988 Asterisks indicate abnormally strong immunoreactivity of MBP at Cpz 3 wks. Scale
989 bars, 500 μm for MBP, CD11c, and Iba1, 100 μm for Olig2. (**B, C**) Areas with
990 demyelination at Cpz 5 wks (**B**) and microgliosis at Basal, Cpz 3-5 wks, and Rec 2 wks
991 (**C**) in the alveus (**alv**) were quantified by the immunoreactivity of MBP and Iba1,

992 respectively. Data are the means ± SEM. A total of 8 areas in 4 images obtained from 4
993 mice (**Cpz 5 wks**), or a total of 4 areas in 2 images obtained from 2 mice (**Basal, Cpz 3**
994 **wks, Rec 2 wks**) were analysed for each genotype. $^{*}P < 0.05$, $^{**}P < 0.01$, $^{***}P < 0.005$
995 (Student's *t*-test). (**D**) The number of Olig2$^{+}$ oligodendrocytes were quantified in the
996 corpus callosum (**cc**). Data are the means ± SEM. A total of 10 images were obtained
997 from 4 mice (**Cpz 5 wks**), or a total of 8 images were obtained from 2 mice (**Basal, Cpz**
998 **3 wks, Rec 2 wks**) and analysed for each genotype. $^{\S\S}P < 0.01$ for Ctrl mice, $^{\dagger\dagger\dagger}P <$
999 0.005 for cKO mice (Student's *t*-test) versus the basal value of respective genotypes. No
1000 statistical significance was found between the two genotypes.

1001 **Supplementary file 1: Gene expression changes in the white matter of CD47 KO**
1002 **mice.** All genes changed more than 2-fold (|Log2 ratio| > 1) in the white matter of
1003 CD47 KO mice were listed. **probe set ID#:** Affymetrix probe set ID number for Mouse
1004 430 2.0 Genome Arrays, **gene:** gene description, **symbol:** gene symbol, **accession:**
1005 NCBI accession number, **Log2 ratio:** fold change expressed as Log2 (KO/WT).
1006
1007 **Supplementary file 2: Gene expression changes in the white matter of CD47 KO**
1008 **mice.** All genes changed more than 2-fold (|Log2 ratio| > 1) in the brain mononuclear
1009 cells of CD47 KO mice were listed. **probe set ID#:** Affymetrix probe set ID number for
1010 Mouse 430 2.0 Genome Arrays, **gene:** gene description, **symbol:** gene symbol,
1011 **accession:** NCBI accession number, **Log2 ratio:** fold change expressed as Log2
1012 (KO/WT).

Fig. 1
Hashimoto *et al.*

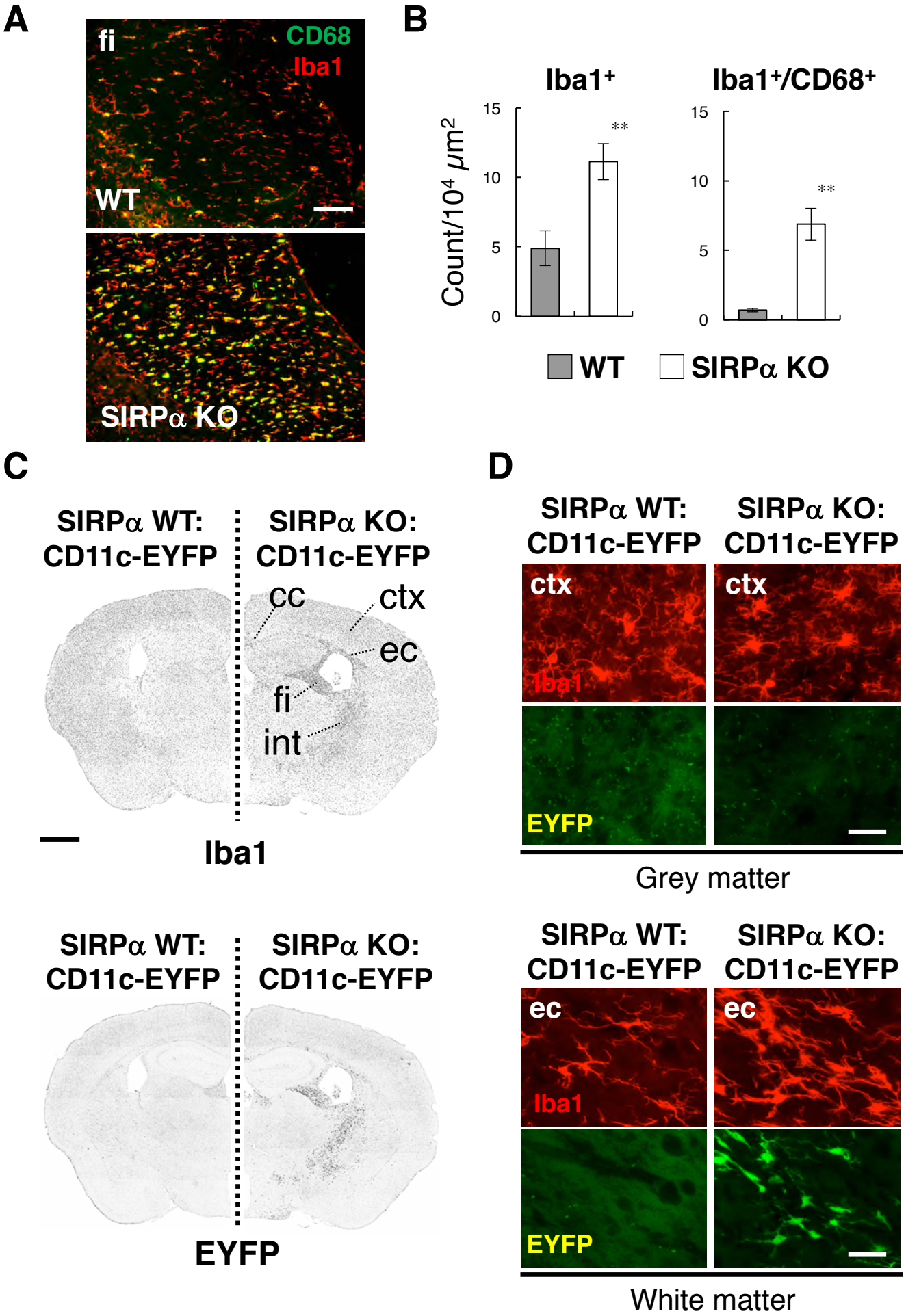

Fig. 2
Hashimoto *et al.*

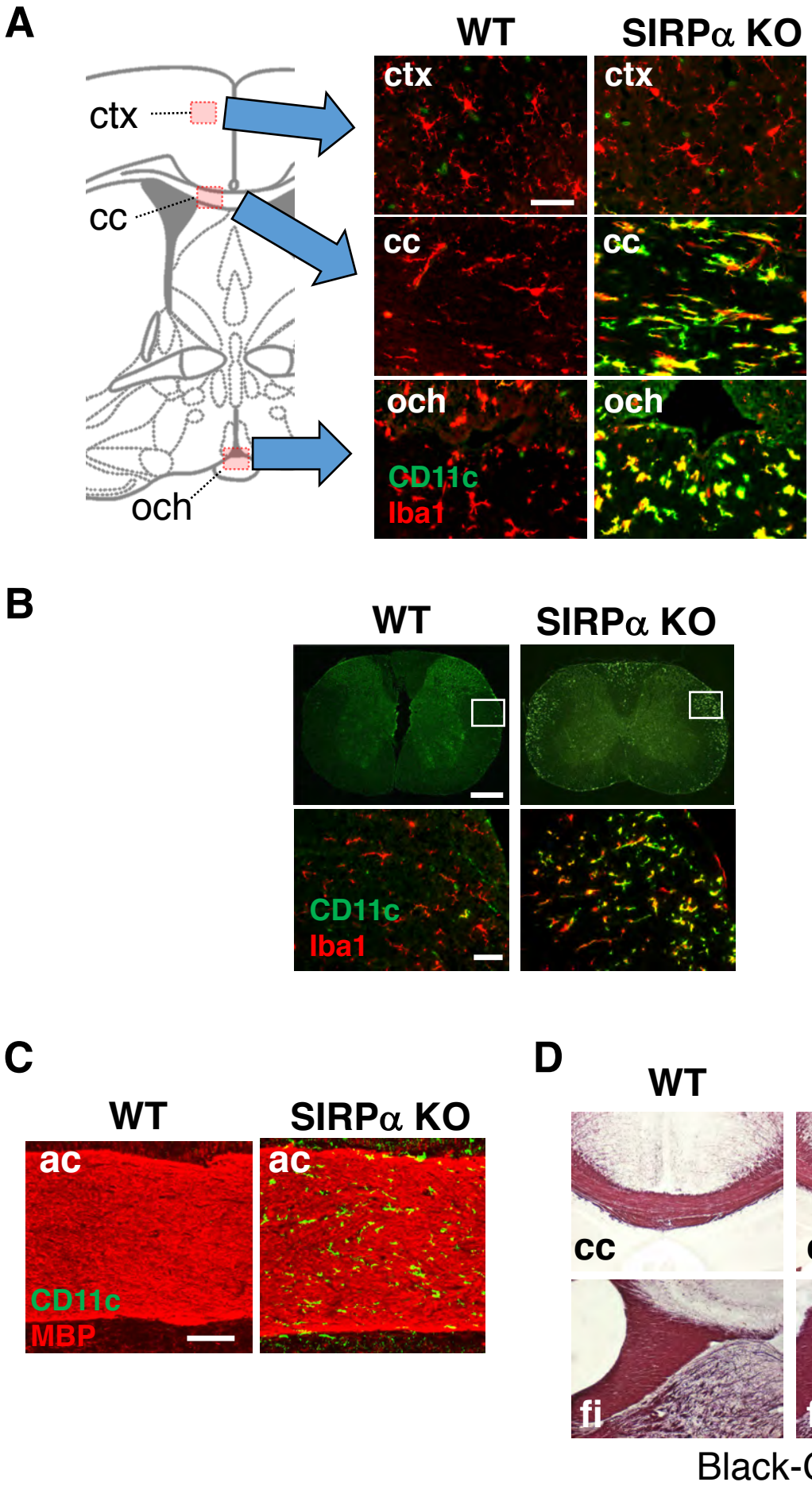

Fig. 3
Hashimoto *et al.*

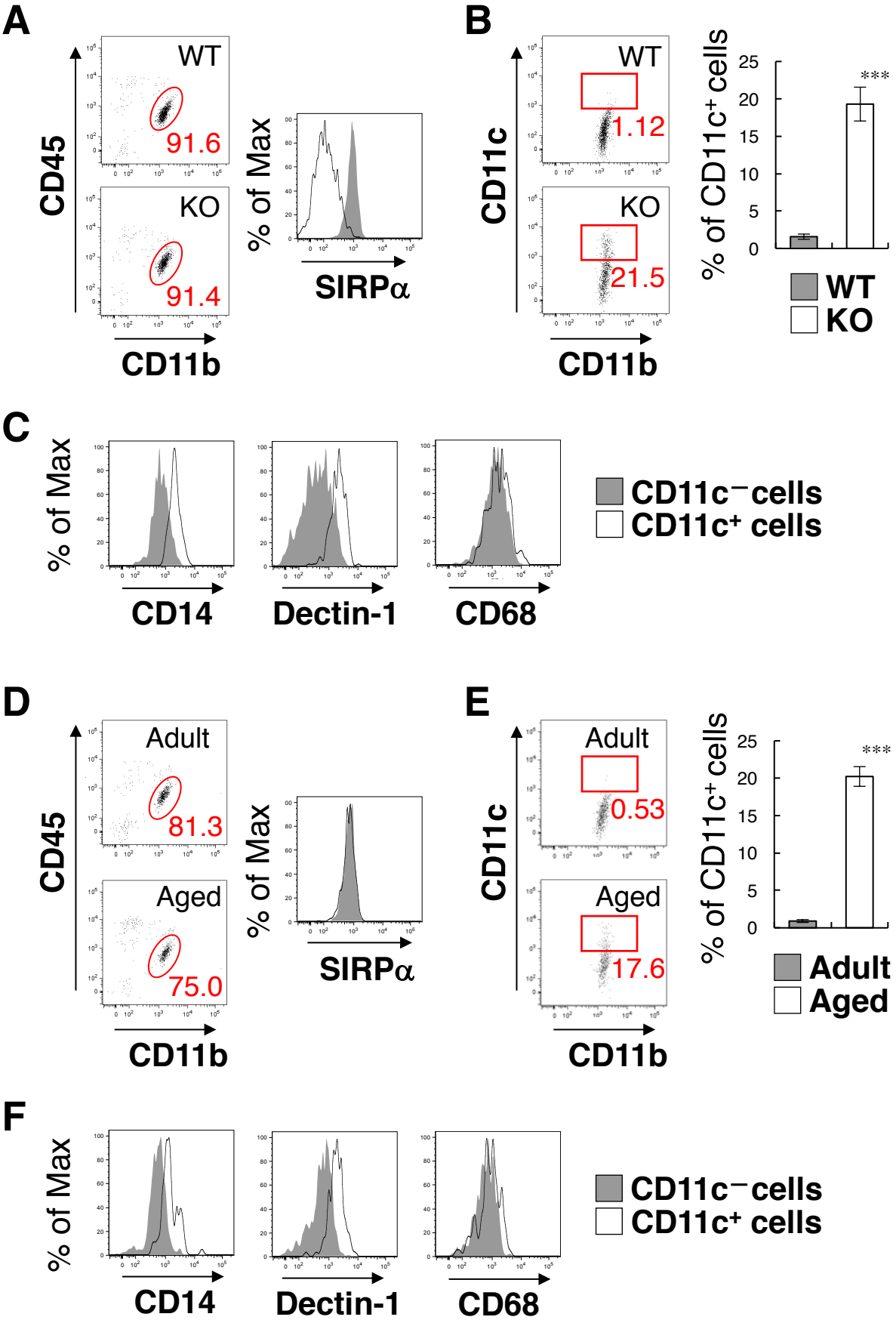

**Fig. 3—figure supplement 1**
**Hashimoto *et al.***

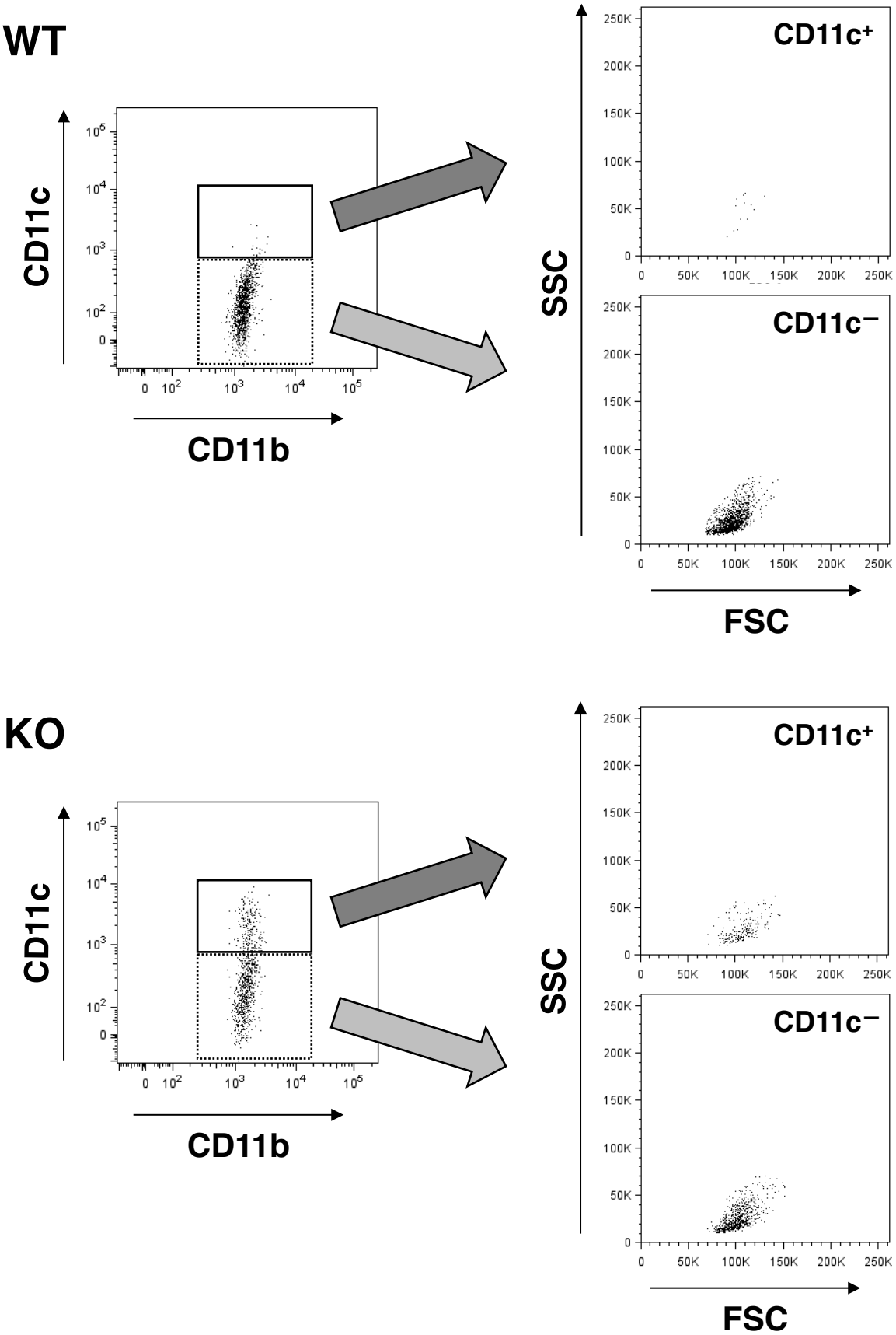

**Fig. 3—figure supplement 2**
**Hashimoto *et al.***

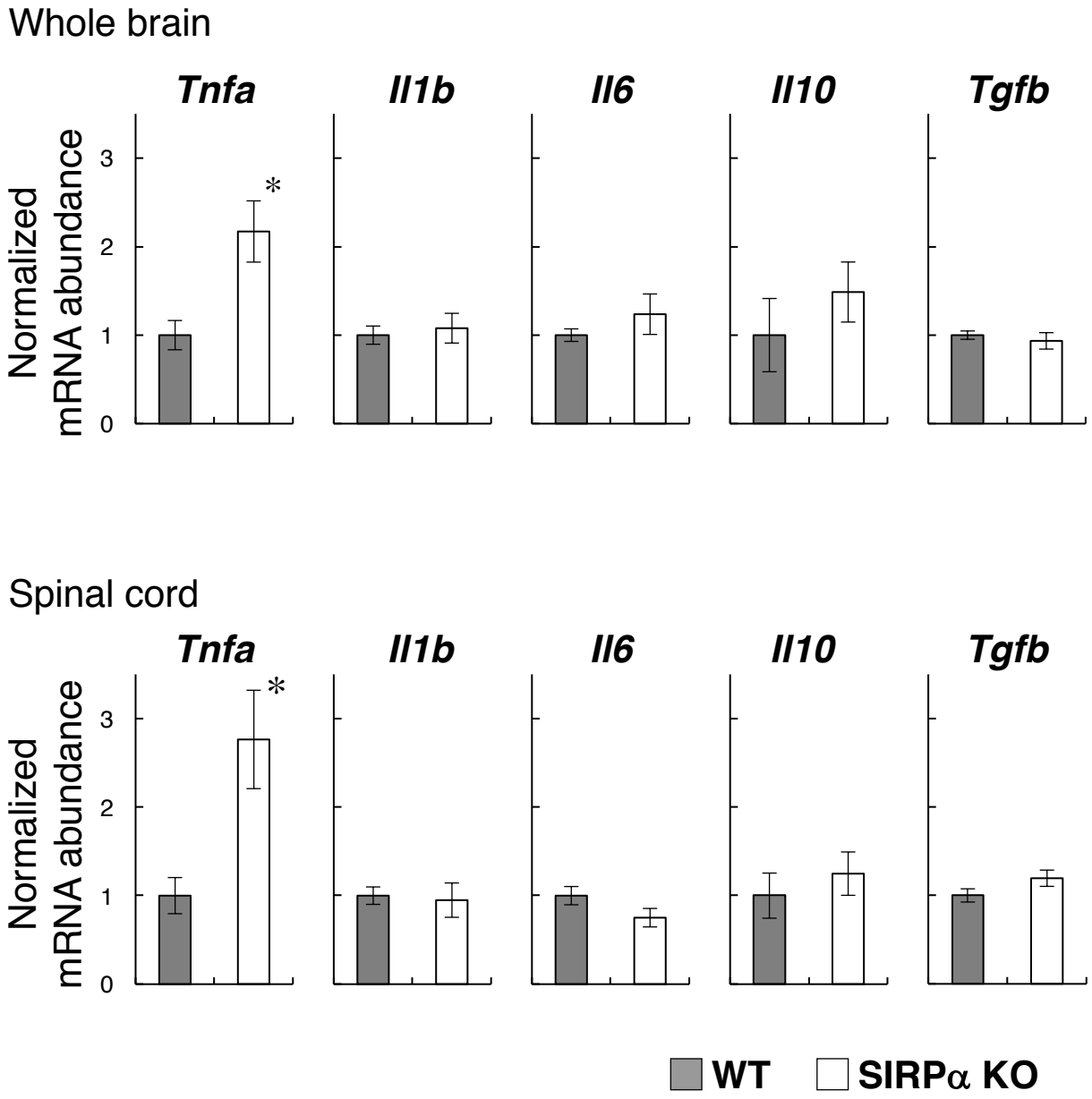

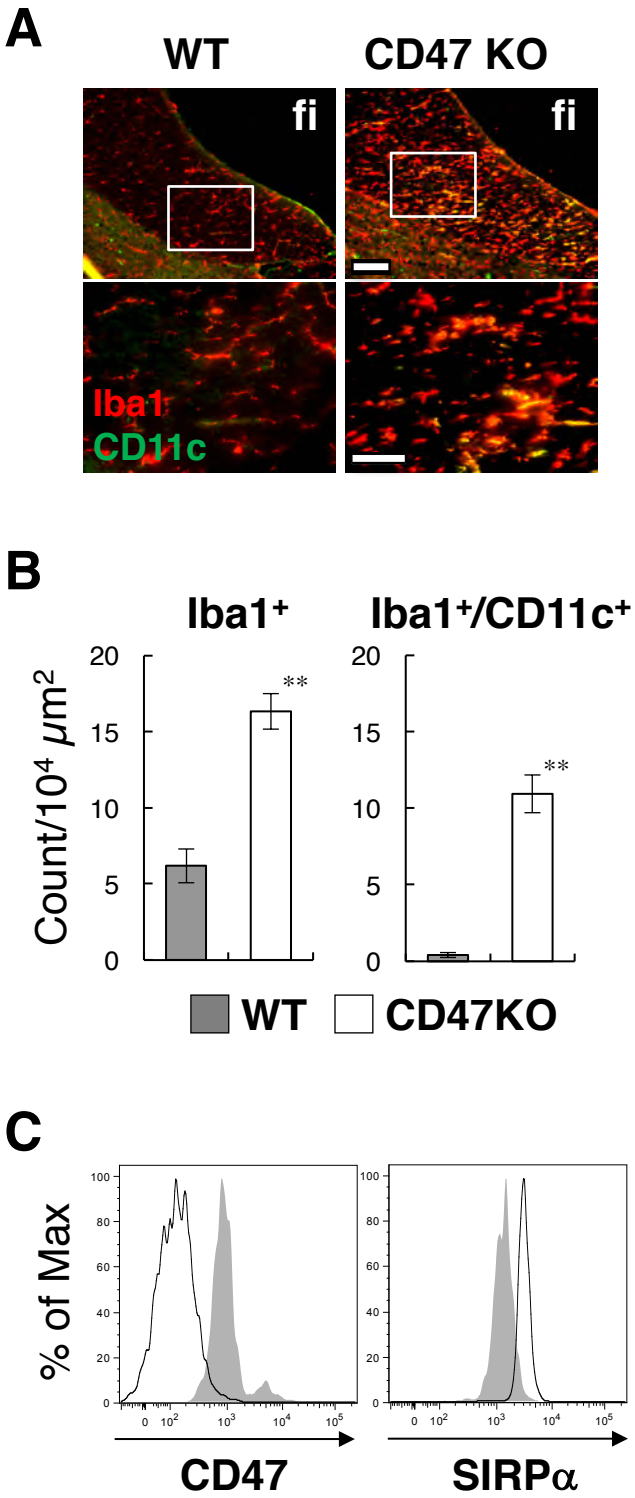
A
WT
CD47 KO
fi
fi
Iba1
CD11c
B
Iba1+
Iba1+/CD11c+
Count/10^4 μm^2
20
15
10
5
0
**
**
WT
CD47KO
C
% of Max
100
80
60
40
20
0
0
10^2
10^3
10^4
10^5
CD47
SIRPα

Fig. 5
Hashimoto *et al.*

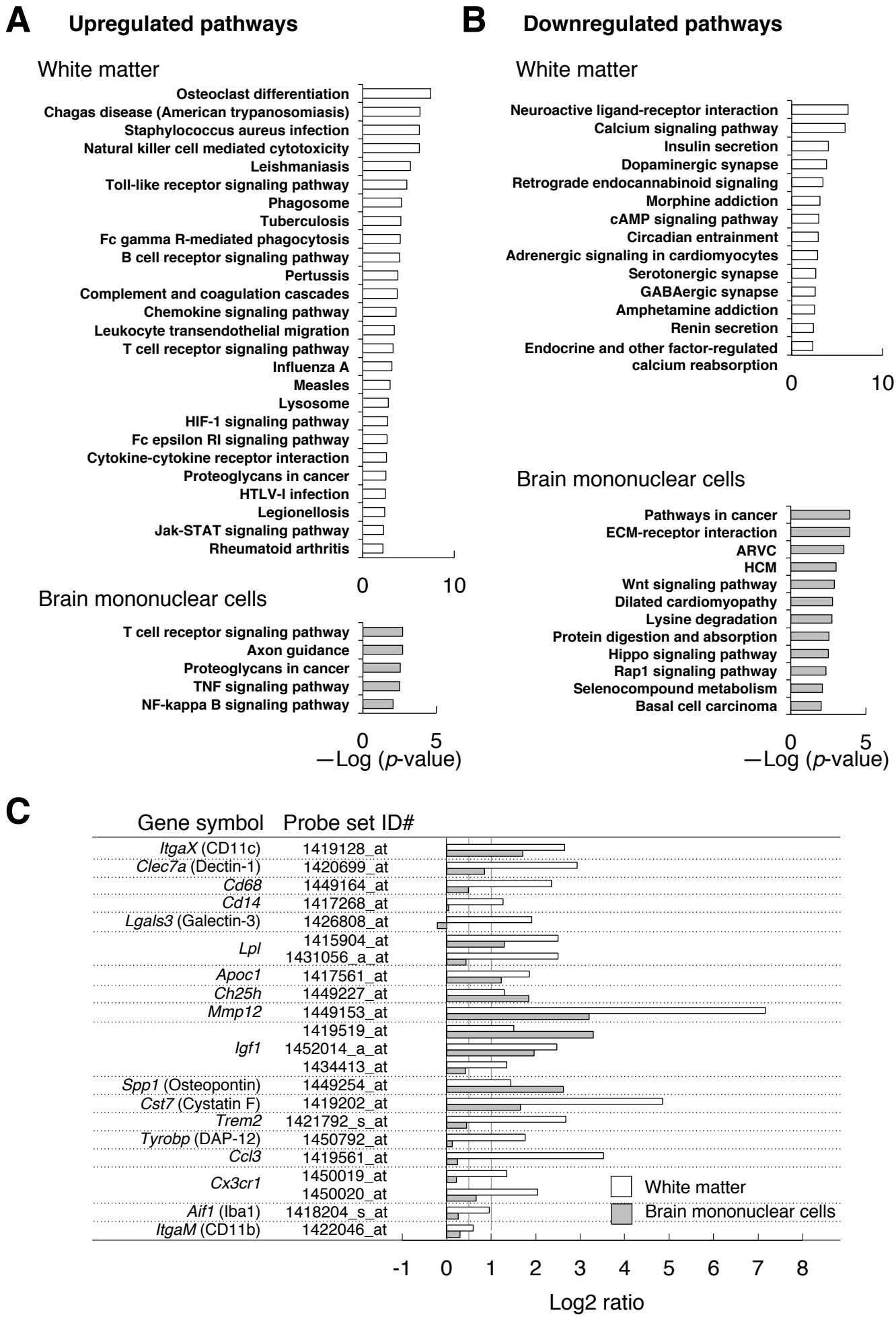

**Fig. 5—figure supplement 1**
**Hashimoto *et al.***

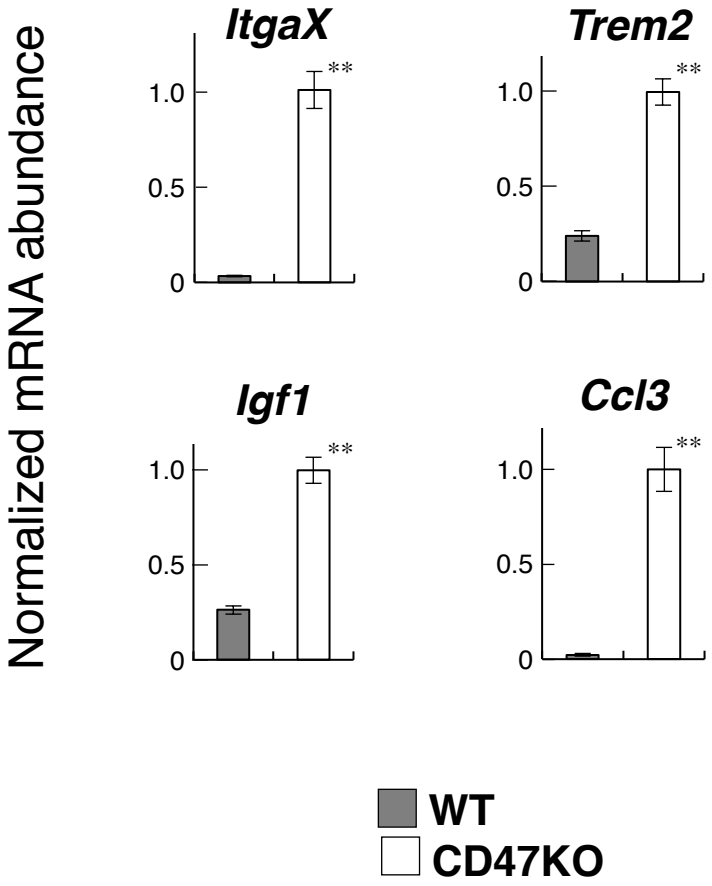

# Fig. 5—figure supplement 2
# Hashimoto *et al.*

**Figure 5—figure supplement 2: Genes commonly changed in both the white matter and the brain mononuclear cells of CD47 KO mice**
Genes (probe sets) commonly changed in both of the white matter and the brain mononuclear cells of CD47 KO mice ( > 2-fold: |Log2 ratio| > 1) were listed.
Expression of total 139 genes were changed in both of the white matter and the brain mononuclear cells of CD47 KO mice.
32 genes (34 probe sets) and 55 genes (58 probe sets) were markedly (> 2-fold) increased and decreased, respectively, in the CD47 KO mice.

| column name | description |
|---|---|
| probe set ID# | Affymetrix probe set ID number for Mouse 430 2.0 Genome Arrays |
| gene | gene description |
| symbol | gene symbol |
| accession | NCBI accession number |
| Log2 ratio | fold change expressed as Log2 (KO/WT) |

## Commonly increased genes

| | | | | Log2 ratio | |
|---|---|---|---|---|---|
| probe set ID# | gene | symbol | accession | whtie matter | brain mononuclear cells |
| 1449153_at | matrix metallopeptidase 12 | Mmp12 | BC019135 | 7.2 | 3.20 |
| 1419202_at | cystatin F (leukocystatin) | Cst7 | NM_009977 | 4.9 | 1.65 |
| 1437244_at | growth arrest-specific 2 like 3 | Gas2l3 | BB770972 | 1.7 | 1.73 |
| 1455980_a_at | growth arrest-specific 2 like 3 | Gas2l3 | BB770972 | 3.1 | 3.87 |
| 1422066_x_at | killer cell lectin-like receptor subfamily B member 1B | Klrb1b | AF342896 | 3.4 | 1.71 |
| 1419519_at | insulin-like growth factor 1 | Igf1 | NM_010512 | 1.5 | 3.29 |
| 1452014_a_at | insulin-like growth factor 1 | Igf1 | AF440694 | 2.5 | 1.97 |
| 1448303_at | glycoprotein (transmembrane) nmb | Gpnmb | NM_053110 | 2.6 | 2.75 |
| 1419128_at | integrin alpha X | Itgax | NM_021334 | 2.6 | 1.71 |
| 1424975_at | sialic acid binding Ig-like lectin 5 | Siglec5 | AF293371 | 2.6 | 1.47 |
| 1449254_at | secreted phosphoprotein 1 | Spp1 | NM_009263 | 1.4 | 2.62 |
| 1415904_at | lipoprotein lipase | Lpl | BC003305 | 2.5 | 1.29 |
| 1427963_s_at | retinol dehydrogenase 9 | Rdh9 | BE979765 | 1.1 | 2.30 |
| 1429667_at | POU domain, class 4, transcription factor 1 | Pou4f1 | BB465134 | 1.6 | 2.28 |
| 1455416_at | Riken cDNA C130021I20 gene | C130021I20Rik | AW209204 | 1.7 | 2.18 |
| 1454043_a_at | potassium voltage-gated channel, shaker-related subfamily, beta member 1 | Kcnab1 | AK015412 | 2.0 | 1.60 |
| 1441214_at | exophilin 5 | Exph5 | BQ176550 | 1.2 | 1.90 |
| 1417561_at | apolipoprotein C-I | Apoc1 | NM_007469 | 1.9 | 1.23 |
| 1449227_at | cholesterol 25-hydroxylase | Ch25h | NM_009890 | 1.3 | 1.85 |
| 1445854_at | RIKEN cDNA C230004F18 gene | C230004F18Rik | BB380166 | 1.2 | 1.79 |
| 1434974_at | pyruvate dehydrogenase kinase, isoenzyme 1 | Pdk1 | BB391928 | 1.6 | 1.72 |
| 1425274_at | aspartate-beta-hydroxylase | Asph | AF289490 | 1.7 | 1.16 |
| 1443757_x_at | ankyrin repeat and zinc finger domain containing 1 /// galactosidase, beta 1-like | Ankzf1 /// Glb1l | BB518847 | 1.1 | 1.65 |
| 1435917_at | OCIA domain containing 2 | Ociad2 | BM937735 | 1.1 | 1.62 |
| 1446130_at | microRNA 1931 | Mir1931 | AW557530 | 1.6 | 1.41 |
| 1418477_at | matrilin 1, cartilage matrix protein | Matn1 | NM_010769 | 1.6 | 1.11 |
| 1426026_at | PRP6 pre-mRNA splicing factor 6 homolog (yeast) | Prpf6 | BC025030 | 1.0 | 1.55 |
| 1431705_a_at | mucolipin 2 | Mcoln2 | AK014467 | 1.2 | 1.42 |
| 1418350_at | heparin-binding EGF-like growth factor | Hbegf | L07264 | 1.2 | 1.08 |
| 1430847_a_at | cAMP responsive element modulator | Crem | AK015641 | 1.1 | 1.37 |
| 1426597_s_at | intermediate filament family orphan 2 | Iffo2 | BG066466 | 1.3 | 1.18 |
| 1449937_at | endonuclease, polyU-specific | Endou | AI528824 | 1.1 | 1.25 |
| 1444692_at | EST AI316844 | AI316844 | BB295954 | 1.2 | 1.23 |
| 1435830_a_at | RIKEN cDNA 5430435G22 gene | 5430435G22Rik | AV293314 | 1.0 | 1.22 |

## Commonly decreased genes

| | | | | Log2 ratio | |
|---|---|---|---|---|---|
| probe set ID# | gene | symbol | accession | whtie matter | brain mononuclear cells |
| 1425799_at | flavin containing monooxygenase 4 | Fmo4 | AF461145 | -4.55 | -5.60 |
| 1445339_at | cyclic nucleotide gated channel alpha 4 | Cnga4 | AV380874 | -4.58 | -1.38 |
| 1418549_at | glycoprotein hormones, alpha subunit | Cga | NM_009889 | -1.32 | -4.01 |
| 1452001_at | nuclear factor, erythroid derived 2 | Nfe2 | L09600 | -3.85 | -1.15 |
| 1442032_at | cDNA sequence BC030500 | BC030500 | AV328055 | -1.30 | -3.79 |
| 1445606_a_at | RIKEN cDNA 2900009J06 gene | 2900009J06Rik | BB663189 | -3.34 | -2.22 |
| 1453631_at | syntaxin 8 | Stx8 | AK011376 | -1.17 | -2.97 |
| 1433404_at | RIKEN cDNA 4930423O20 gene | 4930423O20Rik | AK015192 | -2.93 | -1.05 |
| 1434851_s_at | crumbs homolog 3 (Drosophila) | Crb3 | AU015319 | -2.93 | -1.16 |
| 1435370_a_at | carboxylesterase 1D | Ces1d | AI315015 | -1.20 | -2.66 |
| 1441681_at | exportin, tRNA (nuclear export receptor for tRNAs) | Xpot | C79645 | -1.38 | -2.62 |
| 1439056_at | predicted gene 9866 | Gm9866 | AV331361 | -1.34 | -2.59 |
| 1440370_at | ATP-binding cassette, sub-family A (ABC1), member 13 | Abca13 | BB277120 | -1.10 | -2.58 |
| 1446519_at | RIKEN cDNA A730091E23 gene | A730091E23Rik | BB259739 | -1.24 | -2.48 |
| 1433108_at | T cell receptor beta, variable 1 | Trbv1 | AK018014 | -1.06 | -2.47 |
| 1460150_at | RIKEN cDNA 6330409D20 gene | 6330409D20Rik | BE979371 | -1.71 | -2.44 |
| 1419196_at | hepcidin antimicrobial peptide | Hamp | NM_032541 | -1.24 | -2.42 |
| 1419972_at | solute carrier family 35, member A5 | Slc35a5 | C86506 | -2.26 | -2.14 |
| 1447480_at | fibroblast growth factor 14 | Fgf14 | BB801162 | -2.23 | -1.43 |
| 1459760_at | NADH dehydrogenase (ubiquinone) Fe-S protein 4 | Ndufs4 | BE852624 | -1.13 | -2.10 |
| 1421106_at | jagged 1 | Jag1 | AA880220 | -1.04 | -2.07 |
| 1430997_at | CD47 antigen (Rh-related antigen, integrin-associated signal transducer) | Cd47 | AI882525 | -2.06 | -1.78 |
| 1428187_at | CD47 antigen (Rh-related antigen, integrin-associated signal transducer) | Cd47 | AK018679 | -1.54 | -1.45 |
| 1449507_a_at | CD47 antigen (Rh-related antigen, integrin-associated signal transducer) | Cd47 | NM_010581 | -1.36 | -1.86 |
| 1419554_at | CD47 antigen (Rh-related antigen, integrin-associated signal transducer) | Cd47 | NM_010581 | -1.34 | -1.61 |
| 1432424_at | nudix (nucleoside diphosphate linked moiety X)-type motif 12, opposite strand | Nudt12os | AK015703 | -1.05 | -1.91 |
| 1453540_at | RIKEN cDNA 5430404G13 gene | 5430404G13Rik | BM218780 | -1.91 | -1.87 |
| 1449571_at | thyrotropin releasing hormone receptor | Trhr | M59811 | -1.86 | -1.69 |
| 1427867_at | uncharacterized LOC102633540 /// predicted gene 12300 | LOC102633540 /// Gm12300 | AJ002522 | -1.77 | -1.34 |
| 1456441_at | coiled-coil domain containing 87 | Ccdc87 | BB667164 | -1.74 | -1.38 |
| 1447584_s_at | myc target 1 | Myct1 | AI642973 | -1.08 | -1.74 |
| 1444842_at | lysine (K)-specific demethylase 5A | Kdm5a | BG076005 | -1.30 | -1.73 |
| 1454303_at | epsin 2 | Epn2 | BB626346 | -1.16 | -1.72 |
| 1425005_at | killer cell lectin-like receptor subfamily C, member 1 | Klrc1 | AF106008 | -1.04 | -1.67 |
| 1448076_at | Ctr9, Paf1/RNA polymerase II complex component, homolog (S. cerevisiae) | Ctr9 | BG079166 | -1.65 | -1.38 |
| 1440777_x_at | prostaglandin F receptor | Ptgfr | BB559010 | -1.29 | -1.53 |
| 1418480_at | pro-platelet basic protein | Ppbp | NM_023785 | -1.35 | -1.52 |
| 1442810_x_at | sodium channel, voltage-gated, type IX, alpha | Scn9a | BB452274 | -1.00 | -1.52 |
| 1442282_at | vomeronasal 2, receptor 84 | Vmn2r84 | BB232180 | -1.48 | -1.29 |
| 1431236_at | serine/threonine kinase 32B | Stk32b | BB387845 | -1.13 | -1.37 |
| 1430242_at | RWD domain containing 1 | Rwdd1 | AV356665 | -1.25 | -1.33 |
| 1435891_x_at | RIKEN cDNA 2610021A01 gene | 2610021A01Rik | BQ175465 | -1.02 | -1.29 |
| 1451751_at | DNA-damage-inducible transcript 4-like | Ddit4l | AF335325 | -1.29 | -1.17 |
| 1446215_at | zinc finger homeobox 2, opposite strand | Zfhx2os | AV347642 | -1.28 | -1.29 |
| 1444046_at | shisa homolog 7 (Xenopus laevis) | Shisa7 | AI853734 | -1.25 | -1.20 |
| 1418751_at | suppression inducing transmembrane adaptor 1 | Sit1 | NM_019436 | -1.25 | -1.23 |
| 1442042_at | predicted gene, 20324 | Gm20324 | BG092211 | -1.24 | -1.20 |
| 1423353_at | cysteine-rich secretory protein LCCL domain containing 1 | Crispld1 | BE693025 | -1.22 | -1.14 |
| 1458431_at | eukaryotic translation initiation factor 4, gamma 2 | Eif4g2 | BB159664 | -1.21 | -1.10 |
| 1443143_at | fibronectin leucine rich transmembrane protein 1 | Flrt1 | BB039519 | -1.15 | -1.19 |
| 1418858_at | aldehyde oxidase 3 | Aox3 | NM_023617 | -1.07 | -1.19 |
| 1439620_at | carbonic anhydrase 13 | Car13 | AI326425 | -1.02 | -1.15 |
| 1458472_at | regulatory associated protein of MTOR, complex 1 | Rptor | BB827636 | -1.01 | -1.14 |
| 1424367_a_at | homer homolog 2 (Drosophila) | Homer2 | AB017136 | -1.11 | -1.11 |
| 1422117_s_at | KH domain containing, RNA binding, signal transduction associated 2 | Khdrbs2 | NM_133235 | -1.10 | -1.07 |
| 1415894_at | ectonucleotide pyrophosphatase/phosphodiesterase 2 | Enpp2 | BC003264 | -1.04 | -1.09 |
| 1418156_at | potassium voltage-gated channel, Isk-related subfamily, gene 4 | Kcne4 | NM_021342 | -1.05 | -1.08 |
| 1452456_at | nuclear receptor interacting protein 2 | Nrip2 | BE653335 | -1.06 | -0.65 |

Fig. 6
Hashimoto *et al.*

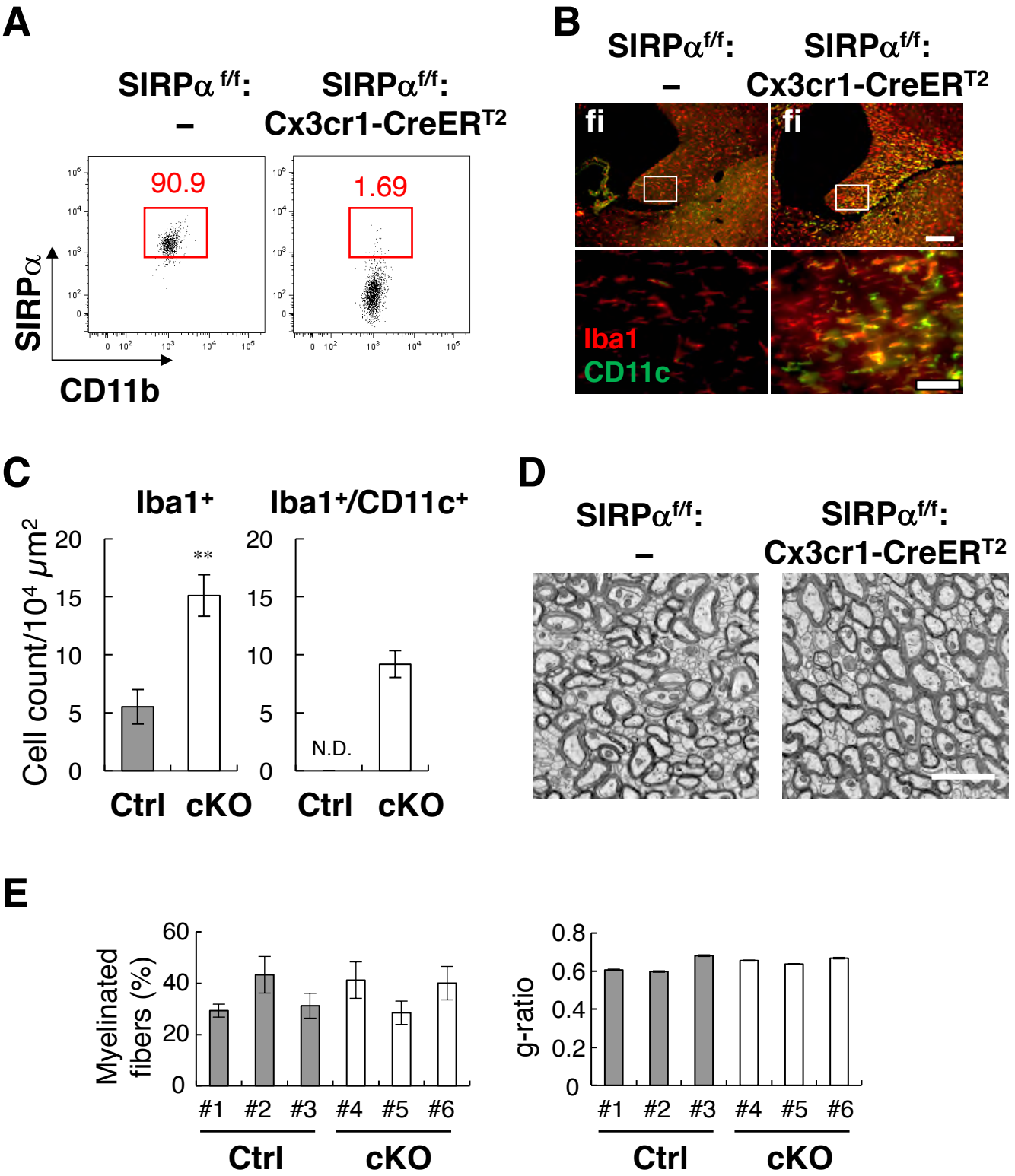

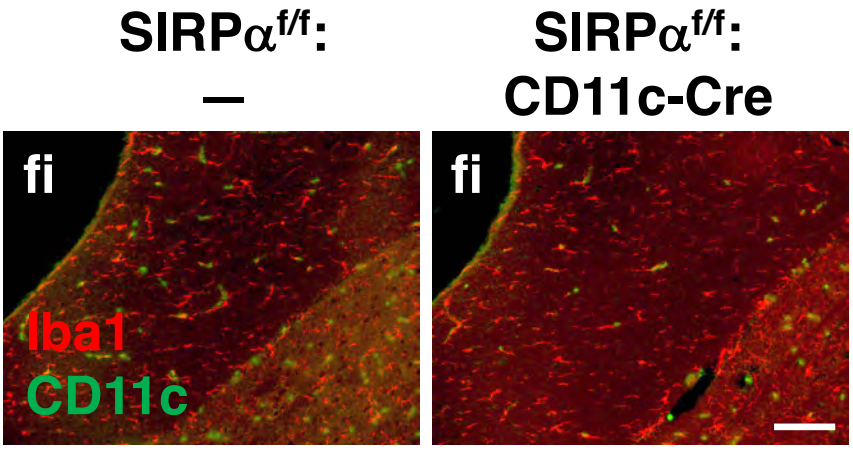
SIRPα$^{f/f}$:
—
SIRPα$^{f/f}$:
CD11c-Cre
fi
Iba1
CD11c
fi
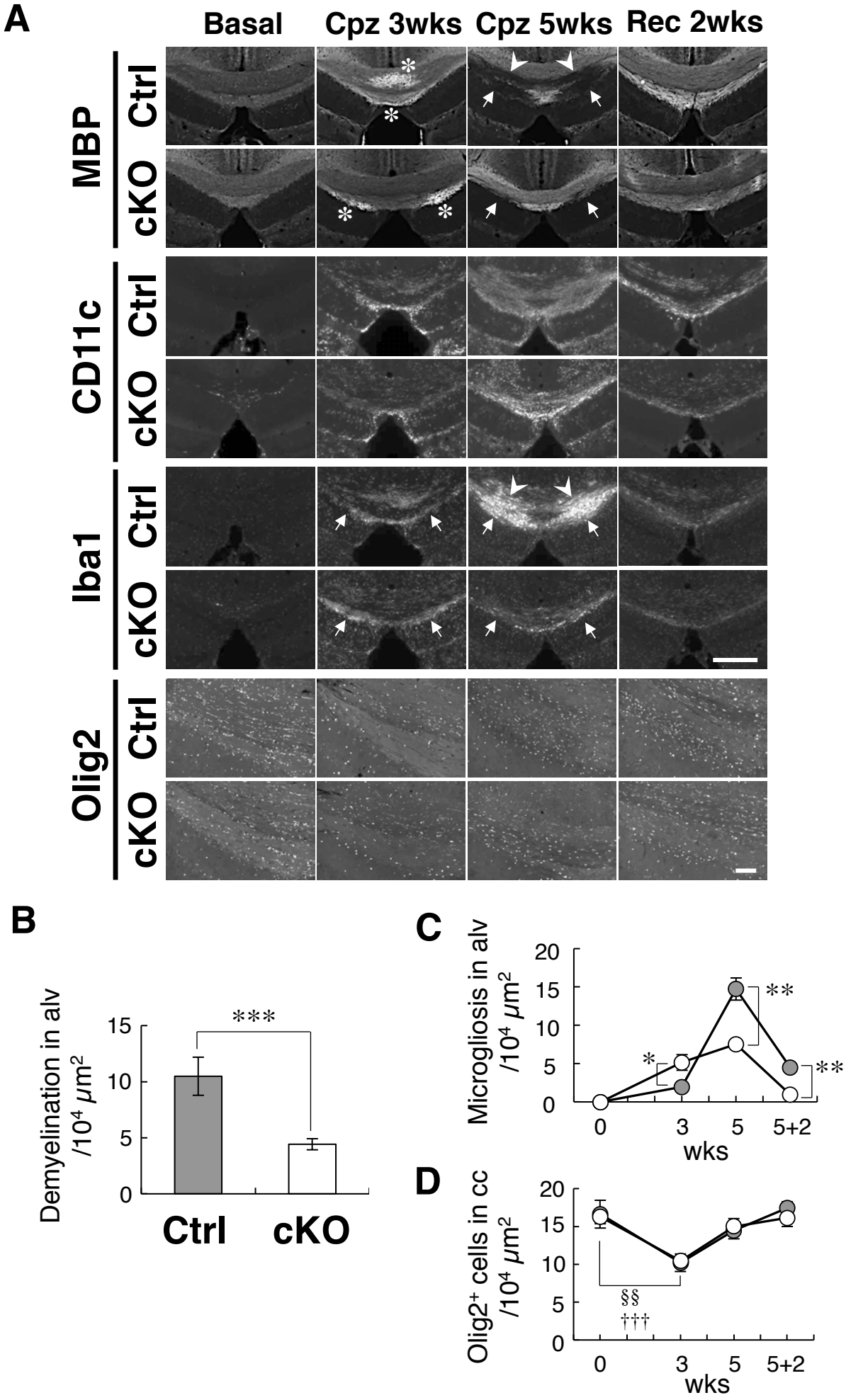
Fig. 7
Hashimoto *et al.*